DESIGN OF A SAFEGUARDS INSTRUMENT FOR PLUTONIUM QUANTIFICATION IN AN ELECTROCHEMICAL REFINING SYSTEM

A Thesis

by

ANNABELLE GAELLE LE COQ

Submitted to the Office of Graduate Studies of
Texas A&M University
in partial fulfillment of the requirements for the degree of

MASTER OF SCIENCE

Chair of Committee,	William S. Charlton
Committee Members,	Sean M. McDeavitt
	Joseph B. Natowitz
Head of Department,	Yassin A. Hassan

August 2013

Major Subject: Nuclear Engineering

ABSTRACT

There has been a strong international interest in using pyroprocessing to close the fast nuclear reactor fuel cycle and reprocess spent fuel efficiently. To commercialize pyroprocessing, safeguards technologies are required to be developed. In this research, the use of Self-Interrogation Neutron Resonance Densitometry (SINRD) has been investigated as a method to safeguard the process and more precisely quantify the ^{239}Pu content of pyroprocessing materials. This method uses a detector array with different filters to isolate the low-energy resonance in ^{239}Pu neutron fission cross section. The relative response of the different detectors allows for the quantification of the amount of ^{239}Pu in the pyroprocessing materials.

The Monte-Carlo N-Particle (MCNP) code was used to design a prototype SINRD instrument. This instrument is composed of a neutron source pod and a SINRD detector pod. Experimental measurements were also performed to validate the MCNP model of the instrument. Based on the results from simulations and experiments, it has been concluded that the MCNP model accurately represents the physics of the experiment. In addition, different SINRD signatures were compared to identify which of them are usable to determine the fissile isotope content. Comparison of different signatures allowed for reduction in the uncertainty of the ^{239}Pu mass estimate. Using these signatures, the SINRD instrument was shown to be able to quantify the ^{239}Pu content of unknown pyroprocessing materials suitable for safeguards usage.

ACKNOWLEDGEMENTS

I would like to thank my committee chair, Dr. William Charlton, for the opportunity he gave me to work on this research project and for his advice and support without which this work could not have succeeded. He provided me an interesting subject and made it more valuable by allowing me to perform an experimental part. I also would like to thank my committee members, Dr. Sean McDeavitt and Dr. Joseph Natowitz for their time and support.

Many thanks go to Dr. Alexander Solodov, Dr. Craig Marianno, and Dr. Braden Goddard and Chris Crouch for their time and help to perform the experimental part of this project. In addition, I would like to thank Bill Averyt, Conner Brazil and Chris King for their effort to build the source system and the SINRD prototype. I must also thank Dr. Sunil Chirayath for his availability to share his expertise with the MCNP code.

Finally, I would like to acknowledge my friends and family who have always encouraged me in my studies. I would like to specifically thank my friends and colleagues Kevin Dugan, Alexandra Khudoleeva, and Marc-Olivier Delchini. They have provided great help during this work and had also made my Master degree a very appreciable and memorable experience.

NOMENCLATURE

ANL	Argonne National Laboratory
BWR	Boiling Water Reactor
C/E	Calculated to Experimental
DA	Destructive Analysis
DCC	Digital Cloud Chamber
EBR-II	Experimental Breeder Reactor II
FC	Fission Chamber
FFM	Fast Flux Monitor
FP	Fission Products
IAEA	International Atomic Energy Agency
IFR	Integral Fast Reactor
INL	Idaho National Laboratory
JAEA	Japan Atomic Energy Agency
KAPF	Korean Advanced Pyroprocessing Facility
LCC	Liquid Cadmium Cathode
LWR	Light Water Reactor
MCNP	Monte-Carlo N-Particle
MOX	Mixed Oxides
NDA	Non-Destructive Analysis
PWR	Pressurized Water Reactor
SINRAD	Self-Indication Neutron Resonance Absorption Densitometry
SINRD	Self-Interrogation Neutron Resonance Densitometry
SNL	Sandia National Laboratory
SQ	Significant Quantity
SSW	Surface Source Write
TRU	Transuranic
UHMWPE	Ultra High Molecular Weight Polyethylene

TABLE OF CONTENTS

Page

LIST OF FIGURES

Page

LIST OF TABLES

Page

1. INTRODUCTION

1.1. Motivations

The electrochemical refining system, or pyroprocessing, was originally developed at Argonne National Laboratory (ANL) in the 1960s. Idaho National Laboratory (INL), active in the development of pyroprocessing, emerged from the combination of Argonne National Laboratory-West (ANL-West) with the Idaho National Engineering and Environmental Laboratory. Under ANL's Integral Fast Reactor (IFR) program, the Experimental Breeder Reactor-II (EBR-II) was built in Idaho. Pyroprocessing was a component of the IFR program and was used to perform the fuel recycle functions for the IFR. The IFR program was terminated in 1994, but the fuel in the reactor core at the time was considered to be unsuitable for long-term geologic disposal without some form of stabilization [1]. This stabilization is necessary due to the sodium heat transfer medium in EBR-II fuel assemblies, which is highly reactive with water. Pyroprocessing was deemed the most attractive option to achieve this stabilization as it was able to provide compact on-site spent fuel separations and fuel fabrication, an efficient handling of sodium bonding, critically-safe conditions for processing highly enriched fuel, and a robust method for processing high burnup fuel avoiding organic solvents [2]. Currently, most research on pyroprocessing is focused on the capability to close the advanced fuel cycle and on commercialization [1, 3].

Several other countries have shown interest in pyroprocessing. India has expressed its preference toward pyroprocessing to perform the processing of their fast reactor spent fuel [4]. South Korea has an important research and development program for pyroprocessing and is more precisely working in collaboration with the USA on the usability of pyroprocessing for spent oxide fuel from light water reactors [1, 5]. The Central Research Institute of the Electric Power Industry (CRIEPI) in Japan is developing pyrochemical reprocessing for inter alia removing residual actinide elements from aqueous reprocessing waste [6]. As another example of this worldwide interest for pyroprocessing, the Commisariat à l'Energie Atomique (CEA) in France is participating

in a research program with 34 partners from Europe, Japan, and Australia to investigate the advantages of the process [7, 8]. Each country working on pyroprocessing has specific applications envisioned depending on their national program: the treatment of thermal reactor spent fuel to recycle actinides in fast reactors, the closure of the fast reactor fuel cycle, and/or nuclear waste management. Besides their different perspectives, the pyroprocessing community has shown interest in an international collaboration to improve the development of the process [9].

Research about pyroprocessing has led to the conclusion that this technique presents the advantage to recycle actinides from high burnup spent nuclear fuel cooled for shorter times and at lower cost than the existing Plutonium and URanium EXtraction Process (PUREX) which is an aqueous process. In addition, pyroprocessing uses relatively small equipment which makes it suitable for use in relatively compact facilities. Another advantage of this process is that less waste is produced and fewer criticality accidents are possible since pyroprocessing is a non-aqueous process. The process has some proliferation resistance advantages due to the highly radioactive materials and high temperatures used in the hot cells, and to the fact that pure plutonium (Pu) is never individually separated in the process [9, 10, 11, 12].

To globally capitalize on these advantages, the commercialization of pyroprocessing requires several improvements: increase of the throughput, enhancement of its remote operability, optimization of the process, waste minimization [13, 14, 15] and the development of safeguards. This safeguards requirement has been stated by the National Nuclear Security Administration's (NNSA) Next Generation Safeguards Initiative (NGSI) to fulfill the International Atomic Energy Agency (IAEA) requirements [5]. The main objective of the IAEA is "the timely detection of diversion of significant quantities of nuclear material from peaceful nuclear activities to the manufacture of nuclear weapons or of other nuclear explosive devices or for purpose unknown, and deterrence of such diversion by the risk of early detection" [16]. A "significant quantity" (SQ) is defined by the IAEA as the approximate amount of nuclear material for which the possibility of manufacturing a nuclear explosive device cannot be

excluded. For Pu, one SQ corresponds to 8 kg by element [17]. The spent fuel material used in pyroprocessing is an IAEA concern since it contains Pu, a direct use nuclear material[1] [17], which may be attractive for an adversary willing to build a nuclear weapon. The IAEA has estimated the time required to convert Pu to the metallic components of a nuclear explosive device (conversion time) in order of 1-3 months [17]. Therefore the IAEA establishes certain frequency of inspections (timeliness goal[2]) to be able to detect the diversion of 1 SQ of nuclear material. In the case of Pu in an irradiated form this goal is 3 months [17]. As examples from 6% Pu MOX spent fuel, only 1.08 Boiling Water Reactor (BWR) assemblies (9x9) and 0.36 Pressurized Water Reactor (PWR) assemblies (17x17) are necessary to be diverted to get one SQ of Pu [18]. Consequently, the quantity of Pu handled by pyroprocessing facilities represents hundreds of SQ. Thus, it is important to effectively safeguard pyroprocessing facilities. However, safeguards for pyroprocessing is complicated by the lack of an input accountability tank (IAT) and the difficulty associated with direct measurement of Pu in solid spent fuel. This has led to interest in research to develop new methods for safeguards applicable to a pyroprocessing facility.

In summary, pyroprocessing presents several advantages compared to the current reprocessing technologies, especially for closing fast reactors fuel cycle. Its attractiveness has driven international research to improve the process. As a large amount of Pu is present in the spent fuel treated by pyroprocessing, safeguards instruments have to be developed to meet the IAEA requirement for Pu quantification in

---

[1] A direct use material is a "nuclear material that can be used for the manufacture of nuclear explosive devices without transmutation or further enrichment. It includes plutonium containing less than 80% ^{238}Pu, high enriched uranium and ^{233}U. Chemical compounds, mixtures of direct use materials [e.g. mixed oxide (MOX)], and plutonium in spent reactor fuel fall into this category." [17]

[2] The IAEA timeliness detection goal is "the target detection times applicable to specific nuclear material categories. These goals are used for establishing the frequency of inspections and safeguards activities at a facility or a location outside facilities during a calendar year, in order to verify that no abrupt diversion has occurred." [17]

order to commercialize the process. Currently, safeguards instruments for pyroprocessing are still under research and untested.

1.2. Pyroprocessing Process

Pyroprocessing is a non-aqueous process based on electrochemical separation. The separation of spent fuel elements is performed through molten chloride salt (LiCl-KCl-$PuCl_3$ or LiCl-KCl-UCl_3) electrolytes which are resistant to high levels of radiation and have a high electrical conductivity potential. Contrary to what the name pyroprocessing implies, fire does not appear in this process.[3] However, pyroprocessing uses very high temperatures (>450^{o}C) at each step of the process and operates in hot cells with an inert argon (Ar) atmosphere to prevent oxidation [2]. Pyroprocessing uses high burnup spent fuel cooled for short times: the neutron dose of the transuranic (TRU) product from pyroprocessing is 140 times higher than that of pure Pu from a conventional Light Water Reactor (LWR) spent fuel (40000 MWd/MTU, 1 year cooling) [11].

The electrorefiner is the key operational unit in pyroprocessing. The goal of this unit is to electrolytically separate the actinides, the cladding hulls, bond sodium, and fission products (FP) using temperatures around 450^{o}C. The metallic fuel rods are chopped into short lengths (6-7 mm) and introduced into the basket of the electrorefiner. When a voltage is applied between the basket (which acts as an anode) and a cathode, molten salts transport actinides from the basket to the cathode. A concentration of 2 mol% of actinide chlorides is maintained in the electrorefiner salt to support electrotransport. Depending on the type of cathode used, the potential applied, and the salt concentration, high purity uranium (U) metal only or both U and TRU elements are deposited: a steel cathode is used to recover only U whereas a liquid cadmium cathode (LCC) stabilizes U mixed with TRU metal elements. Figure 1.1 shows the two types of

[3] For this reason, pyroprocessing has more recently adopted the name electrochemical processing.

materials that can come from this process [19, 20]. In the current engineering-scale equipment, approximately 4 kg of Pu and minor actinides with 1 kg of U on the LLC and around 15 kg of U on the solid cathode can be collected. When FP concentration in the salt exceeds pre-specified limits (10 mol%), the salt is sent to the ceramic waste process or is cleaned up and recycled back to the process. At the end of the electrorefining step, metal waste are left in the anode basket, ceramic waste are formed by the salts, and the cathode material will go through a purification step [1, 2, 10, 21].

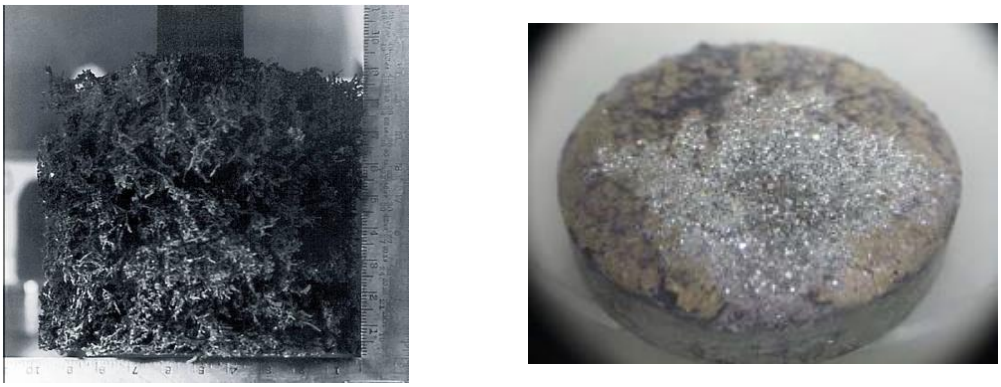

(a) (b)

Figure 1.1. Pyroprocessing materials: (a) dentritic uranium deposit on eletrorefiner cathode, (b) Cd ingot containing actinides

The cathode processor ensures the purification of the actinide deposit formed at the electrorefiner cathode. The salt left over in the deposits is removed by making it boil at around 800°C, and the deposits are cast into a solid ingot using a temperature close to 1,200°C. The technique used in the cathode processor is vacuum distillation [1, 2, 10].

The waste process is divided into two steps both having the mission to concentrate FP into stable waste forms and make the waste suitable for permanent geologic disposal. On one hand, the metal waste furnace processes the cladding and the undissolved fuel left in the anode basket of the electrorefiner as well as noble metal FP (such as technetium, rhodium, and molybdenum). A temperature of 1,600°C is used to

melt the stainless steel-rich alloy of the cladding. The metal is then consolidated into an ingot and is considered as a High-Level Waste (HLW). On the other hand, the ceramic waste processing has the role to immobilize the contaminated salt from the electrorefiner containing cesium, strontium, and rare earth elements. At temperature between 500^{o}C and 900^{o}C, FP combined with zeolite and glass are heated and then cooled into a stainless steel can [1, 2, 10].

Research on pyroprocessing has been adapted to applying the process to spent oxide fuel from commercial LWR in order to recover actinide elements and recycle them to the reactor as fuel materials. Subsequently, a voloxidation step and an oxide reduction step have been investigated to make oxide spent fuel compatible with the electrorefining and the other steps of the original pyroprocessing process. The goal of the voloxidation step is to fully oxidize (and powder) the spent fuel from LWR. Once the spent oxide fuel is completely oxidized, the oxide reduction transforms this spent fuel to a metallic form enabling it to be introduced in the electrorefiner and to undergo further pyroprocessing steps [1, 10, 13]. Figure 1.2 summarizes the pyroprocessing steps into a flow sheet.

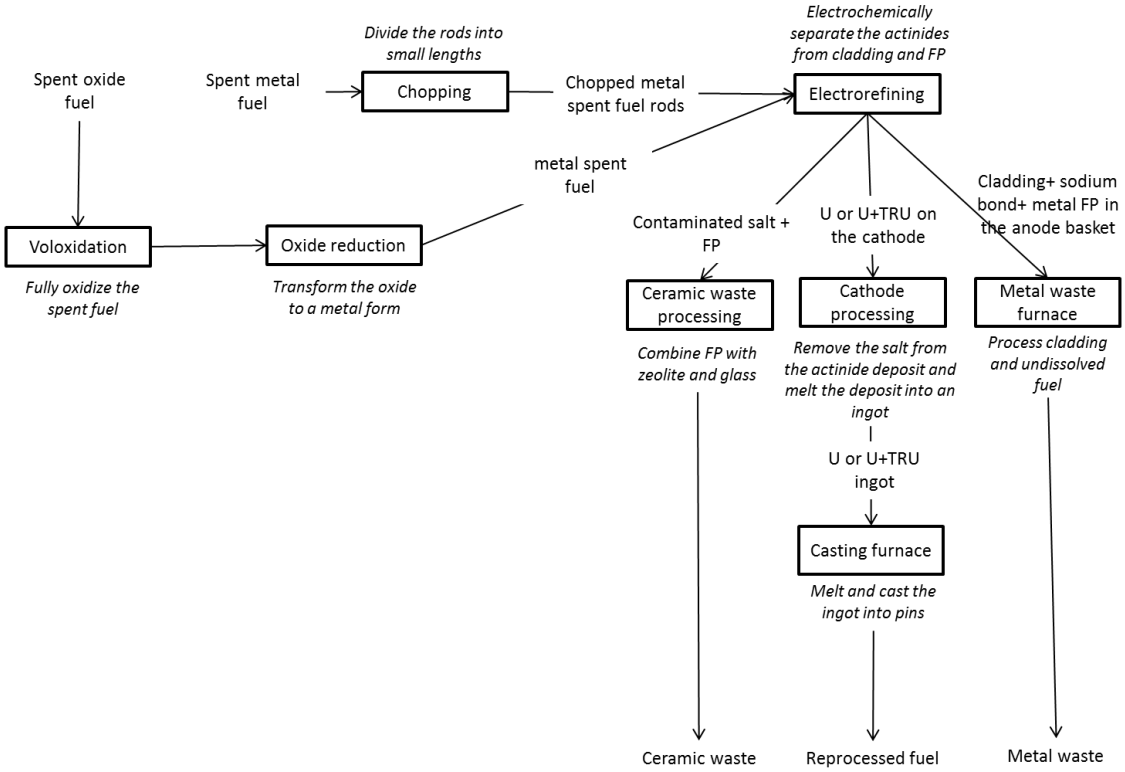

Figure 1.2. Pyroprocessing flow sheet

1.3. Current Study to Safeguard Pyroprocessing

Developing safeguards for pyroprocessing is challenging since there are few pyroprocessing facilities and those that do exist are at national laboratories and not subject to international safeguards. Thus, the process has only been developed at laboratory or pilot-scale, meaning that the quantity of material currently injected in a pyroprocessing facility is smaller than the quantity that would be used commercially. The lack of experience with pyroprocessing and with the assay of nuclear materials in metal or salt solutions by destructive analysis (DA) or nondestructive analysis (NDA), make the development of a safeguards technology more difficult. The materials containing Pu in pyroprocessing facilities are very different from current reprocessing facilities [22]. The difficulty to safeguard pyroprocessing comes also from the hot cell environment. A hot cell is a shielded nuclear radiation containment chamber which

contains high-temperature, high-radiation fields and is difficult to access for maintenance. High temperature salt and metal solutions are highly corrosive. These constraints make the development of an instrument for measuring within the hot cell difficult [5, 23, 24].

1.3.1. Gross neutron counts

INL had first investigated the use of gross neutron counting to follow the materials containing Pu throughout the process and quantify Pu. This method has been inconclusive in measuring Pu as the spent nuclear fuel also contains curium (Cm) - a significant neutron emitter. Thus, the gross neutron counts are mostly attributed to ^{244}Cm (and not Pu).

A neutron balance (Cm accounting) method consists of measuring the gross neutron counts at several steps of pyroprocessing: at the input of the process, at the electrorefiner, at the casting, and at the output of the process. It would be possible to deduce the amount of Pu in the process by determining through NDA or DA the Pu to Cm ratio and the Cm amount. If the Pu to Cm ratio stays constant through the process, the amount of Pu can be deduced and a measurement of this ratio at the beginning of the process could reveal the contribution of Pu on the neutron emission relative to Cm. However, the difficulty to detect Cm in processed salt has slowed down the development of this method. Also, the inseparability of Pu and Cm would have to be proven and the measured material need to be homogeneous to use this method for safeguards [5, 25, 24].

1.3.2. Digital cloud chamber

The pyroprocessing hot cell environment presents a challenge for NDA of the material due to high-temperature and high-radiation level. INL has been working on pyroprocessing safeguards via diversion pathway analysis, the development of a digital cloud chamber (DCC) along with the inverse spectroscopy algorithm, and Monte-Carlo N-Particle (MCNP) [26] modeling of the detector response around the electrorefiner.

The cloud chamber concept was originally developed by Wilson in 1912 [27]. The device is a sealed container generally filled with supersaturated water or alcohol vapor. When radiation enters the cloud chamber, it ionizes the surrounding atoms and gas molecules condense around these ions. Thus, radiation tracks in the cloud chamber form streaks of mist in the device. The type of radiation and its energy can be identified by analyzing the size, width and length of these streaks. The DCC got its name because of its coupling with two digital cameras. The cameras are placed orthogonally to visualize the radiation track in 3D. The cameras have a 10-megapixel resolution and are equipped with a high speed connection (fiber optics) transmitting data to electronics outside of the hot cell environment. Figure 1.3 [28] shows the design of the instrument (a) and the radiation tracks in a cloud chamber (b). The four pistons shown on the figure ensure a supersaturated vapor by providing a sufficient volume [28].

The DCC has the advantage of not being altered by high temperature and high radiation exposure, to be low cost and to require a small amount of energy (110V/60Hz). INL is demonstrating that the DCC can identify a gamma-ray source in terms of isotope emitter, intensity and location of the source. This system will make it possible to determine if the Pu content of a material is homogeneously distributed and will use an inverse spectroscopy algorithm capable of determining the energy and the spatial origin of a gamma ray. Depending on the energy and spatial resolution of the results, the DCC could be able to quantify Pu in pyroprocessing. The primary goal of the DCC is to confirm that Pu is located where it should be and not anywhere else. Neutron streams in the DCC could also be used, but present more difficulties to analyze due to the low interaction between neutrons and the gas of the DCC. INL had originally developed this system for long term hot cell monitoring before considering its use in pyroprocessing. The disadvantages of the DCC for use in pyroprocessing are that it requires a long counting time, it is a physically large detector (100,000 cm^3), and it is not specific to measuring Pu [5, 28, 29].

(a) (b)

Figure 1.3. Digital Cloud Chamber: (a) Design of the DCC and (b) tracks observed with the instrument

1.3.3. Safeguards by design

The Korea Advanced Pyroprocessing Facility (KAPF) has been used as a conceptual facility to develop a Safeguards By Design (SBD) approach for LWR pyroprocessing. The goal of this approach is to design a new facility taking into account, since the beginning of its design, the safeguards provision and features. This facility was divided into seven Material Balance Areas [4] (MBAs) containing twelve Key Measurement Points[5] (KMPs) where the material flow was analyzed using both NDA and DA with random and systematic uncertainties based on the International Target

[4] A material balance area is "an area in or outside of a facility such that: (a) the quantity of nuclear material in each transfer into or out of each 'material balance area' can be determined; and (b) the physical inventory of nuclear material in each 'material balance area' can be determined when necessary, in accordance with specifier procedures, in order that the material balance for Agency safeguards purposes can be established." [17]

[5] A key measurement point is "a location where nuclear material appears in such a form that it may be measured to determine material flow or inventory. 'Key measurement points' thus include, but are not limited to, the inputs and outputs (including measured discards) and storages in material balance areas." [17]

Value (ITV) 2000 [30]. From the uncertainty in Material Unaccounted For[6] (MFU) evaluation based on a hypothetical operating scenario, it was concluded that a safeguards system for a pyroprocessing facility like KAPF could be designed to meet the IAEA requirements [31, 32]. However, this approach has not been confirmed for usage with pyroprocessing of fast reactor fuel.

NDA techniques investigated by the Korean Atomic Energy Research Institute (KAERI) for accounting for nuclear materials include a passive neutron-based assay accounting for electrolytic-reduction uranium and process materials, active neutron coincidence counting, and gamma-ray spectroscopy measurement. A Passive Neutron Albedo Reactivity (PNAR) counter was designed for direct measurement of fissile content in the process and will be tested in hot cells at INL. A surveillance system composed of neutron monitors, surveillance cameras and motion detection was developed to send monitoring information of the surveillance system to the IAEA and Sandia National Laboratory (SNL) in the U.S. This system was developed not only for nuclear material accountancy and monitoring in pyroprocessing but also for the IAEA remote safeguards verification system [25].

SNL has also created a model of a commercial-scale electrochemical plant using Matlab Simulink. The goal of this model is to design and analyze safeguards and security systems simulating material flow rates, material accountancy and process monitoring measurements [33].

1.4. Self-Interrogation Neutron Resonance Densitometry Method

The term Self-Interrogation Neutron Resonance Densitometry (SINRD) has been used by the IAEA for methods using Self-Indication Neutron Resonance Absorption

---

[6] The material unaccounted for "is calculated for a material balance area over a material balance period using the material balance equation, commonly written as: MUF= (PB+X-Y)-PE where PB is the beginning physical inventory, X is the sum of increases to inventory, Y is the sum of decreases from inventory, PE is the ending physical inventory." [17]

Densitometry (SINRAD) for measurement on spent fuel, using the Cm self-contained neutron source [34]. The SINRAD measurement technique was originally developed in 1968 by Howard Menlove at Los Alamos National Laboratory [35]. In this method, the neutrons issued from spontaneous fission of ^{244}Cm in spent fuel are used to react with the fissile content of spent fuel fulfilling the self-interrogation of the spent fuel. These neutrons will slow down in any moderating material surrounding the spent fuel object. This will produce an interrogation source with a 1/E spectrum of neutrons in the resonance region. This energy distribution about 0.3 eV is a crucial component of the SINRD method as it provides a high neutron flux for the resonance of interest.

The design of SINRD used in previous research [18] uses fission chambers (FC) to detect neutrons. A FC is a neutron detector containing gas and a small layer of fissionable material on the chamber inner wall –usually highly enriched uranium (HEU). The neutrons inducing fission in this fissionable material can be detected indirectly by the fission fragments. The two fragments issued from a fission event travel in opposite directions, i.e. one fragment is absorbed by the wall of the detector and the other enters the gas. Then, the ionization caused by this second fragment in the gas is sensed by the detector. FCs have low neutron detection efficiency and are more sensitive to thermal neutrons. However, FCs have a low sensitivity to gamma rays [36]. Considering that pyroprocessing hot cells are high gamma-ray environments, the FC is the detector type more likely to provide usable neutron output data. In addition, if a large number of neutrons are available for counting, the low efficiency of FCs is not an issue. Thus, SINRD is a candidate to be considered to measure fissile content in pyroprocessing material. Neutron methods are usually preferred for safeguards and accounting because of their high material penetrability compared to gamma rays; gamma rays would only see the exterior part of the measured material.

The SINRD method has been investigated for nuclear safeguards and material accountability measurements and led to the conclusions that: (1) the MCNP model of SINRD accurately simulates the physics of the experiment on fresh fuel assemblies, (2) SINRD requires calibration with a reference material to be insensitive to any

potential sources of bias error, (3) SINRD could accurately quantify ^{239}Pu in BWR and PWR spent low enriched uranium (LEU) and MOX fuel when hafnium (Hf) is added to the Gd filter, and (4) SINRD provides improvements of current IAEA verification methods about burnup and fuel diversion [18].

SINRD is based on isotope cross sections, which describe the likelihood that a neutron of different energies interacts with this isotope. The variations of likelihood of interaction between an isotope and a neutron form resonances in the cross section at specific incident neutron energies. The foundation of SINRD is based on the unique resonance structure in fission cross sections. The sensitivity of this method relies on the use of the same fissile material in the detector as the measured material. For example, ^{239}Pu FCs would be used to measure ^{239}Pu in a sample. As the reaction occurring in the detection process is fission (n,f), the cross section of interest is the (n,f) cross section. The more ^{239}Pu in the sample, the more neutrons with energy corresponding to a resonance will react with the fissile isotope in the sample and then fewer neutrons of the same energy will react with the fissile isotope in the FC [18].

In this research, ^{239}Pu and ^{235}U are the isotopes of interest. These two fissile isotopes both present a resonance in their fission cross-section around 0.3 eV. Figure 1.4 shows their fission cross-sections versus incident neutron energy and emphasizes their resonance at 0.3 eV. Cross section data comes from the Java-based nuclear information software (JANIS) evaluated nuclear data files (ENDF-VII.1) database [37]. The energy window of interest is represented by the black rectangle on the figure. To isolate this resonance for measurement, gadolinium (Gd)-covered and cadmium (Cd)-covered FCs are used. As Gd absorbs neutrons of energy below 0.13 eV, the Gd-covered FC detects neutrons of energy higher than 0.13 eV. Similarly, since Cd absorbs neutrons of energy below 1.25 eV, the Cd-covered FC detects neutrons of energy higher than 1.25 eV. The 0.3 eV resonances from ^{239}Pu and ^{235}U are located in the window formed by Gd and Cd cutoff energies. In addition to these two FCs, a bare FC expected to measure the thermal neutrons and a boron carbide (B_4C) FC complete the detector design. B_4C absorbs neutrons of energy below 3.8 keV. The B_4C FC is expected to measure the fast neutrons

– neutrons above 3.8 keV. In the following, this FC will be called the fast flux monitor (FFM) [18].

Figure 1.5 shows these different FCs in the SINRD instrument designed in previous research [18]. According to the FC used in SINRD, the neutron energy groups are defined as follow: thermal for neutron below 0.13 eV, epithermal for neutron between 0.13 eV and 3.8 keV, and fast for neutrons above 3.8 keV. As the 0.3 eV ^{239}Pu resonance is larger than the 0.3 eV ^{235}U resonance, the self-interrogation effect will be larger for ^{239}Pu than for ^{235}U.

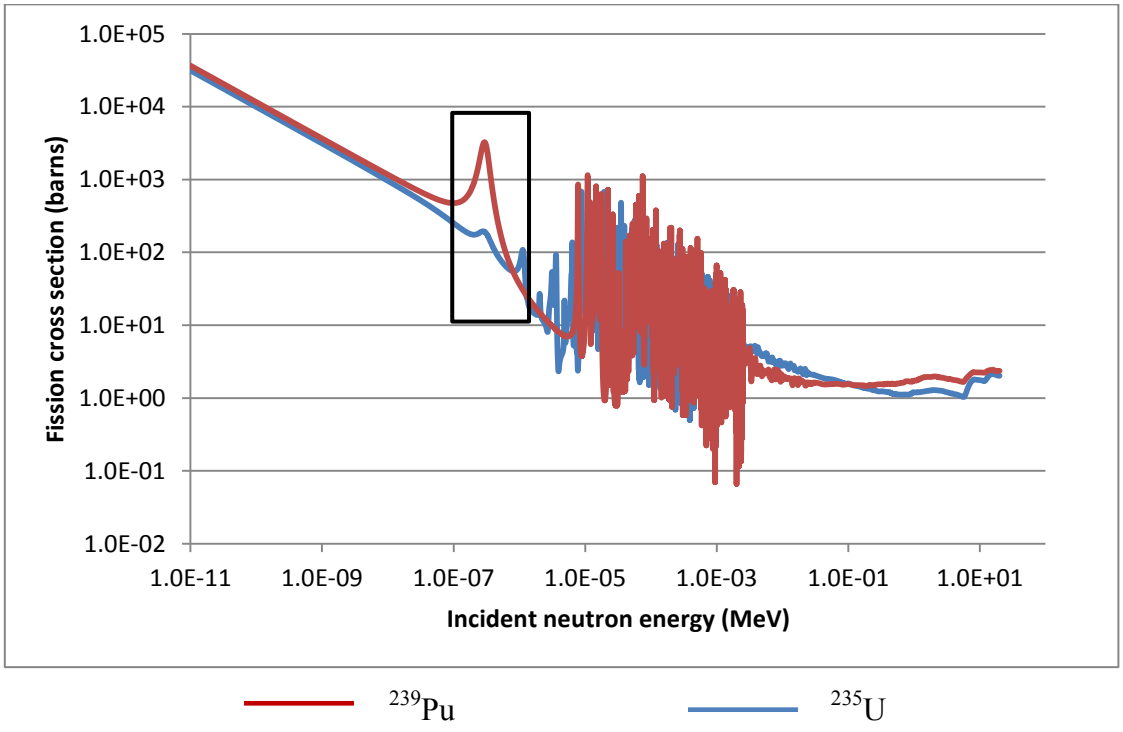

Figure 1.4. Fission cross-sections for ^{235}U and ^{239}Pu

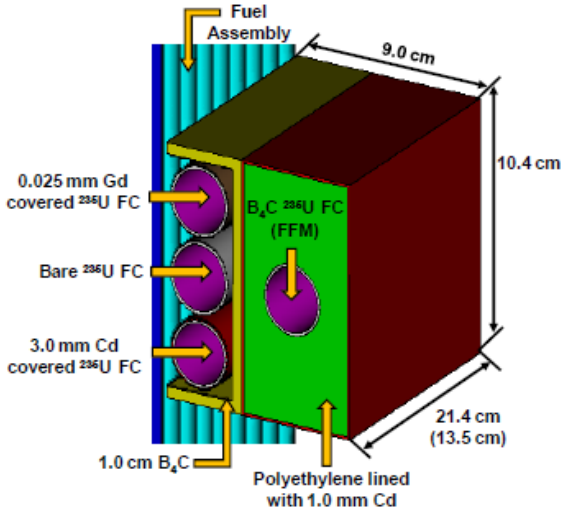

Figure 1.5. SINRD instrument designed in previous research

1.5. Objectives

The primary objective of this research is to design a safeguards instrument that can be used at pyroprocessing facilities, within the hot cells, to quantify the ^{239}Pu content of pyroprocessing materials throughout the process. Online monitoring requiring small counting times is a desired characteristic for this instrument. The ability of SINRD to fulfill this quantification function will be investigated using an existing design of SINRD [18]. The pyroprocessing process investigated in this research is based on the INL Fuel Cycle Facility (FCF) pyroprocess to treat spent fuel from the EBR-II, i.e. metallic fast reactor spent fuel [12, 38].

In order to develop this instrument, MCNP version 5 (MCNP5) [26] and eXtended (MCNPX) transport codes [39] were used to: (1) design a neutron source with the desired neutron energy and spatial distribution, (2) model safeguards relevant materials to be measured (cans of U and ingots of Pu-bearing materials representing a pyroprocessing material), and (3) analyze the ability of SINRD measures to quantify the fissile content of the material.

Due to the restraint about measuring spent fuel, experimental measurements were instead performed on fresh fuel (specifically cans of U_3O_8 powder of varying enrichments) to validate the instrumentation design and its ability to quantify fissile content. In the case of U cans, the ability of the instrument to quantify ^{235}U was tested. As ^{235}U and ^{239}Pu are both fissile isotopes with a resonance around 0.3 eV, the ability of the instrument to quantify ^{239}Pu in spent fuel is expected to be related to its ability to quantify ^{235}U in fresh fuel. Experimental results obtained with FCs as well as ^{3}He tubes in the detector pod were compared. As ^{3}He tubes have a higher efficiency than FCs, the goal of this comparison was to evaluate if the two types of detectors with different efficiency have a similar behavior when the fissile content of the material varies. It is important to remember that ^{3}He tubes could not be used in pyroprocessing hot cells because of their higher sensitivity to gamma rays compared to FCs. These measurements were also compared to MCNP simulations to verify the accuracy of the MCNP instrument model. The results of this research will evaluate the capability of the designed instrument to perform direct measurement of fissile content of pyroprocessing material and determine if the instrument is a suitable candidate to safeguard pyroprocessing facilities. An overview of the MCNP simulations and experimental measurements performed is shown in Figure 1.6.

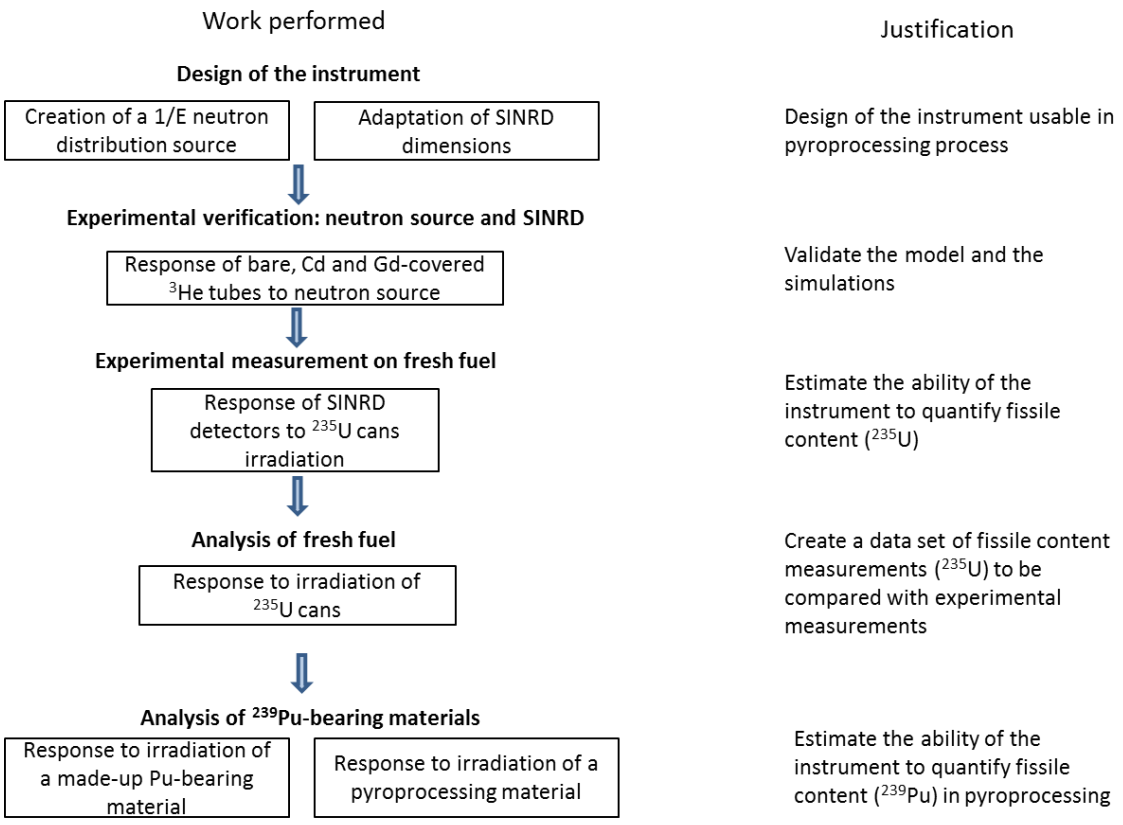

Figure 1.6. Overview of MCNPX simulations and experimental measurements for this research

2. DESCRIPTION OF THE INSTRUMENTATION DEVELOPED

In this research, the instrument was developed through simulations for application in the pyroprocessing process. This process uses spent nuclear fuel as its input and results in Pu and U bearing products potentially mixed with other minor actinides. However, due to constraints on handling spent fuel, the validation experiment for the instrumentation was performed using fresh fuel (specifically U_3O_8 in Al cans). Both fresh and spent fuels present a fissile isotope of interest – respectively ^{235}U and ^{239}Pu. The configuration of the instrumentation used in the experimental part of this research is slightly different compared to the setup used in simulations on spent fuel. The two different configurations of instrumentation are described in this section.

2.1. SINRD Detector Configuration

The SINRD detector configuration used as reference [18] was optimized for LWR and BWR fuel assemblies. The detector unit was rectangular with a width equal to the width of the assembly [18]. The detector configuration for this research has been driven by the dimensions of the pyroprocessing materials of interest. However, the dimensions of the detector used for measurement on fresh fuel have been determined according to the equipment available to perform this experiment. In both cases, the same features as the previous MCNP SINRD design [18] were kept in the detector design: (1) the bare, Gd-covered and Cd-covered fission chambers are placed in aluminum for structural purpose[7]; (2) the FFM is placed in a Ultra High Molecular Weight Polyethylene (UHMWPE) block to thermalize the fast neutrons transmitted through the B_4C to increase the FFM detection efficiency; and (3) the polyethylene is lined by Cd to reduce background from thermal neutrons reentering the detector pod.

[7] Aluminum does not change a neutron energy much as aluminum does not interact strongly with a neutron.

Bare and FFM detectors respectively monitor the thermal and fast flux of the system whereas Gd and Cd detectors are specifically set up to react to fissile content. Thus, the bare and FFM detectors are always U FCs whereas the Gd and Cd FC are made of U or Pu depending on the fissile isotope to quantify. U FCs could be able to record a signature from a Pu sample as both ^{235}U and ^{239}Pu present a low-energy resonance around 0.3 eV. However, the signature using U FCs is expected to be lower than Pu FCs as the low-energy resonance is smaller for ^{235}U than ^{239}Pu. The ^{239}Pu FCs modeled contain 1.5 mg/cm^2 of fissile content – 94 wt% ^{239}Pu metal whose density is equal to 19.8 g/cm^3. All U FCs are 93 wt% ^{235}U metal whose density is equal to 19.1 g/cm^3.

As the electrorefiner is at the center of pyroprocessing, the materials coming from the electrorefiner were used to adjust the SINRD detector dimensions to the process. The two materials produced from the electrorefiner are the uranium deposit on a solid cathode and the actinide deposit on a LLC. Mostly ^{235}U will be found as fissile content in the uranium deposit on the solid cathode whereas ^{239}Pu is the fissile isotope of interest in the LCC. As ^{239}Pu is the main concern for pyroprocessing safeguards, the Cd ingot formed in the LCC is the pyroprocessing material used in this research. However, the instrument developed could be tested to quantify the ^{235}U content of the solid cathode as well. As pyroprocessing is essentially developed on a lab scale, the materials issued from the process have relatively small dimensions. The uranium deposit is about 9-cm high and has a 10-cm diameter including the cathode diameter. The Cd ingot bearing uranium, plutonium and other actinides is 1.67-cm high and has a 2.5-cm diameter [40]. As it would be convenient to have for future prospective only one instrument that can be used throughout the process, the biggest pyroprocessing material determined the dimensions of the SINRD detector for this research (even if only the Cd ingot is used). The detector length was then fixed at 9.4 cm and the width of the detector pod at 12.4 cm. Pu and U FCs were both used with the Gd and Cd filters to prospect the best SINRD signature. Figure 2.1 illustrates the detector configuration with adapted

dimensions for use in pyroprocessing. Only the active length of the FCs has been modeled.

The experiment performed on fresh fuel used ^{235}U FCs to quantify the ^{235}U content of U cans. The results are compared to those from measurements with ^{3}He tubes. Fission counters model 30773 from LND, INC [41] were used for the Gd- and Cd-covered fission chambers and fission counters model 30774 from the same manufacturer were used for the bare FC and FFM. Four same FCs were not available for this experiment: the 30773 FC is ten times more efficient than the 30774 FC. As the Gd and Cd-covered FCs were expected to record the fewest counts, the FCs with the highest efficiency available were used for Gd and Cd-covered detectors to obtain better counting statistics on these chambers. The ^{3}He tubes used were the model 252 cylindrical ^{3}He neutron detectors from LND, INC [41]. One should note that the connector and the electronics have not been modeled in the MCNP models, since these components do not significantly change the physics of the system. As connectors and electronics would add some noise to the system, we expect the MCNP uncertainties are slight underestimates compared to the experimental measurements.

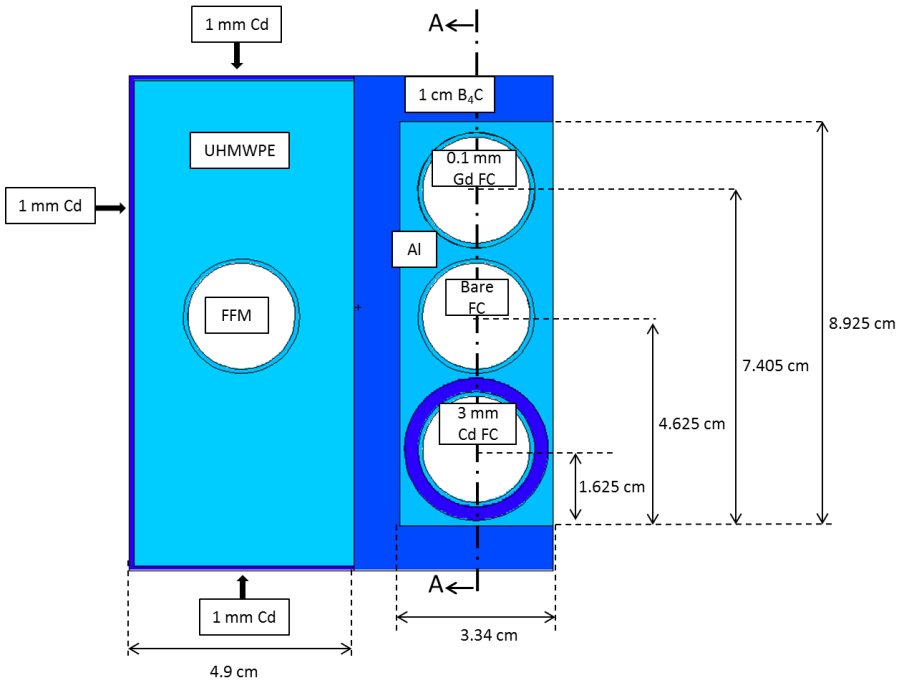

(a)

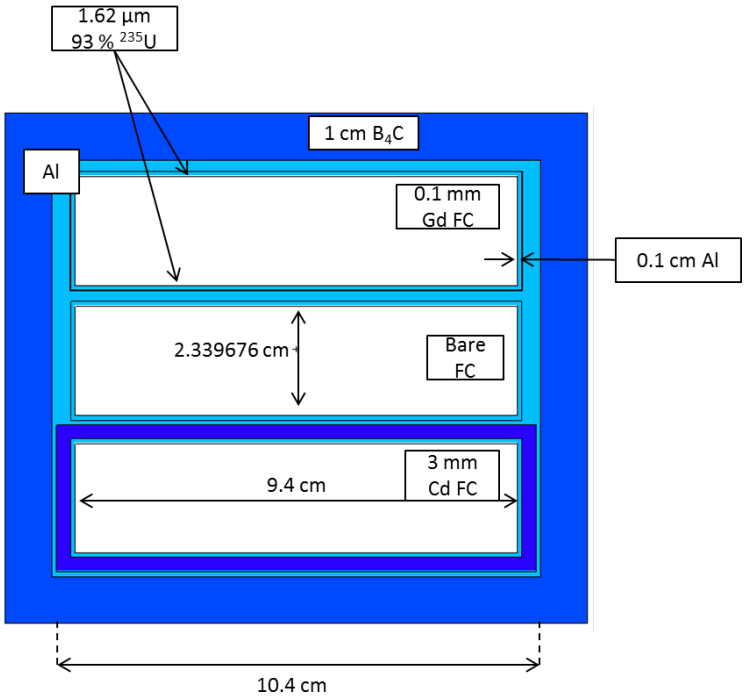

(b)

Figure 2.1. MCNP model of SINRD detector for use in pyroprocessing: (a) top view and (b) A-A cut

The prototype of the experimental SINRD detector pod has been designed in order to keep the same amount and type of materials around the detectors as in previous research [18]: the Al block containing the bare, Cd-, and Gd-covered detectors is 0.201 cm bigger than the detectors length at each detector end; the Cd- and Gd-covered detectors are respectively surrounded by 0.1 cm and 0.24 cm of Al; the UHMWPE block containing the FFM provides 1.08 cm of UHMWPE between the FFM and the B_4C; this block has the same height and width as the Al block surrounded by B_4C powder. All the detectors of the array are located at the same height in the detector pod. In order to contain the B_4C powder, an Al case made of 0.5-cm thick plates was added to the prototype to surround the Al block and powder. The top Al plate has been machined in order to be removable to pack B_4C powder in the detector pod. The natural B_4C powder has been packed into the detector pod at a density of 1.06 g/cm^3; this density could be increased up to 1.45 g/cm^3. The FC and the ^3He tubes chosen have a similar diameter but a different length. The detector pod dimensions were adapted according to the longest detector used for the experiment – the ^3He tube. In addition, holes have been drilled in the detector pod to be able to insert and remove detectors from the pod. Because of these holes in the detector pod, B_4C powder has not been included at the top of the detector pod. To ensure that both FCs and ^3He tubes are located at the center of the detector pod while not changing the configuration of the pod, Styrofoam has been inserted before FCs. The Styrofoam compensates for the length difference between the FC and ^3He tube but does not significantly affect the behavior of neutrons in the detector pod (due to its very low density). Figure 2.2 shows the experimental arrangement of the detector pod used for the experiment. The drawings used for machining of the equipment can be found in Appendix A.

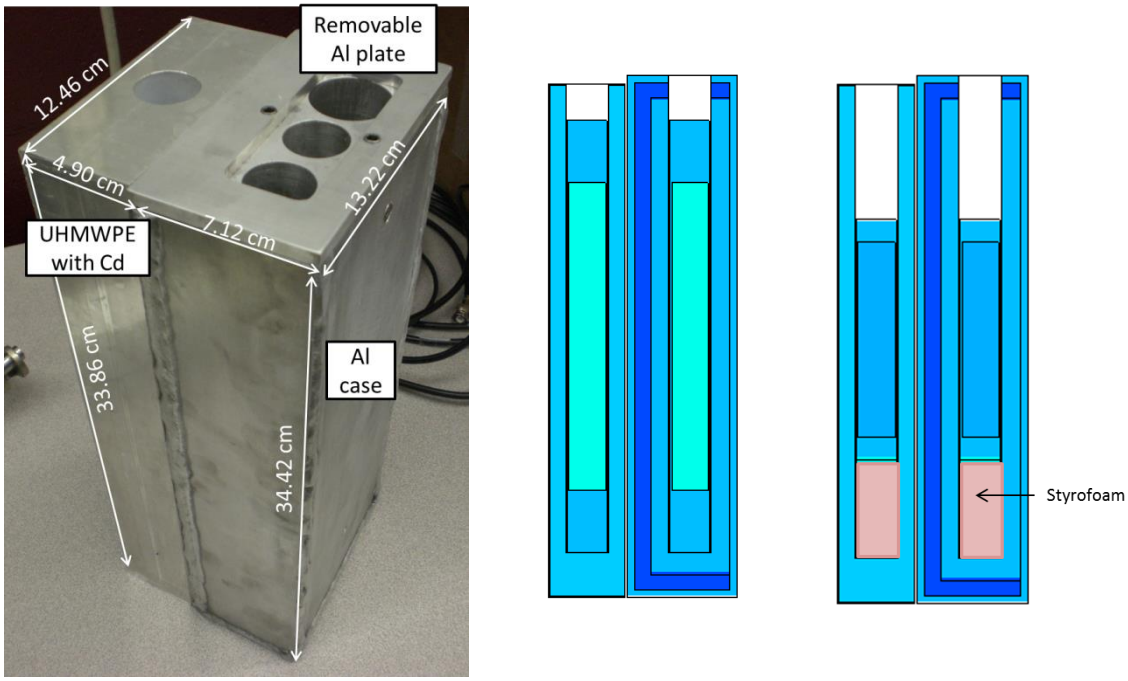

(a) (b) (c)

Figure 2.2. Arrangement of the detector pod for the experiment: (a) dimensions of the detector pod machined for the experiment, (b) MCNP model of ^{3}He tubes inserted in holes and (c) MCNP model of FCs with Styrofoam to maintain FCs at the center of the pod

2.2. Neutron Source

In pyroprocessing, there is not necessarily enough Cm decaying by spontaneous fission to self-interrogate the pyroprocessing material at each step of the process. An external neutron source is then needed to interrogate the item of interest. The neutron source must have a slowing-down energy spectrum, i.e. where the neutron flux is inversely proportional to the neutron energy. This moderated neutron spectrum is especially important to get usable counting statistics in the Cd-covered FC.

Californium-252 (^{252}Cf) was chosen to generate neutrons in this instrument. ^{252}Cf is often used in experiments involving neutrons. This isotope emits neutrons by spontaneous fission. UHMWPE is a well-known moderator, i.e. neutrons scatter in polyethylene and then loose energy. In order to obtain a moderated neutron spectrum,

the ^{252}Cf source was placed in UHMWPE. To generate a neutron source that was more spatially uniform across the front face of the detector pod, two ^{252}Cf sources were placed inside a UHMWPE piece.

The MCNP model of the source is shown in Figure 2.3. The two ^{252}Cf sources were placed at the focal of an ellipsoid shaped block of UHMWPE. The characteristic of the focal of an ellipse is that, for whatever point chosen on the edge of the ellipse, the sum of the distance from each focal point to the edge is a constant. In other terms, each point on the edge of the ellipse is at the same distance from the two sources combined. This leads to a constant source of uncollided neutrons along the ellipse edge. A piece of nickel (Ni) was placed against the polyethylene. Ni is a weak reflector and moderator with a medium atomic mass. It is used in this design to smooth the neutron spectrum. Neutrons mostly scatter with Ni which has a scattering cross-section constant for neutron energy between 0.01 eV and 1 keV. Finally, a thin Gd sheet (0.1 mm thick) was placed on the front side of the neutron source. Consequently, only neutrons above 0.13 eV are emitted by the neutron source preventing fission at low energy in the material to measure. By only transmitting neutrons above 0.13 eV, most of the large ^{239}Pu resonance is utilized. The lower energy neutrons are absorbed by the Gd sheet. They do not contribute to the self-indicating effect and if present, they will decrease the SINRD response [35]. For the MCNP simulations to quantify ^{239}Pu, the source was 2-cm thick with reflective surfaces at the top and bottom to create an infinitely thick source, preventing neutrons from leaking in these two directions.

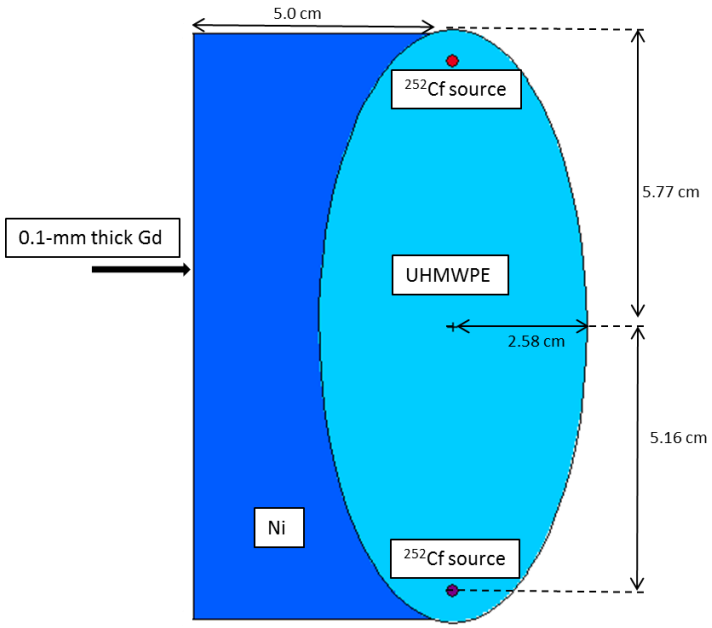

Figure 2.3. MCNP model of the neutron source as seen from above

To better understand the effect of each material used in the source, MCNP tests have been run with the two ^{252}Cf sources and with: (1) no other material, (2) UHMWPE only, (3) UHMWPE and Gd, and (4) UHMWPE, Ni and Gd. The neutron flux was calculated with MCNP at 0.1 cm from the Gd of the source using several energy bins. The energy bins were chosen according to the energies of interest for this problem. That is more energy bins were defined in the Gd-Cd window than at thermal energies as it is expected that Gd absorbs most of the thermal source neutrons. The energy bins are shown in Table 2.1. The neutron flux tallied by MCNP for each energy bin was divided by the bin size. The results are shown in Figure 2.4. The neutron spectrum from the sources alone shows a distribution with mostly fast neutrons. Adding UHMWPE around the sources thermalizes the neutrons and forms a slowing down distribution as well as Maxwellian distribution at thermal energies. Then, the thin Gd sheet absorbs most of the neutrons below 0.13 eV, decreases the neutrons flux at energies above but close to the cutoff (until 0.3 eV) and then leaves unchanged the slowing down distribution obtained

with UHMWPE only. The Gd energy cutoff is shown with a purple line on the figure. Finally, the neutron distribution including the Ni is shown. The Ni provides a slight smoothing to the neutron spatial and energy distribution. This last neutron spectrum has the desirable properties for this research and will be used in the instrument developed. This prototype design of the source has been obtained from different tests modifying the dimensions and shape of the materials to get a slowing down function with the highest neutron flux around the resonance of interest (0.3 eV).

Table 2.1. Energy bins used to calculate the source neutron spectrum

Energy group	Thermal	Epithermal		Fast
		in Gd-Cd window	above Gd-Cd window	
Energy bins (MeV)	[0; 1.0e-8] [1.0e-8; 1.0e-7]	[1.0e-7; 2.0e-7] [2.0e-7; 4.0e-7] [4.0e-7; 0.5e-6] [0.5e-6; 0.8e-6] [0.8e-6; 1.0e-6] [1.0e-6; 1.0e-5]	[1.0e-5; 1.0e-4] [1.0e-4; 1.0e-3]	[1.0e-3; 1.0e-2] [1.0e-2; 1.0e-1] [1.0e-1; 1] [1; 1.0e+1]

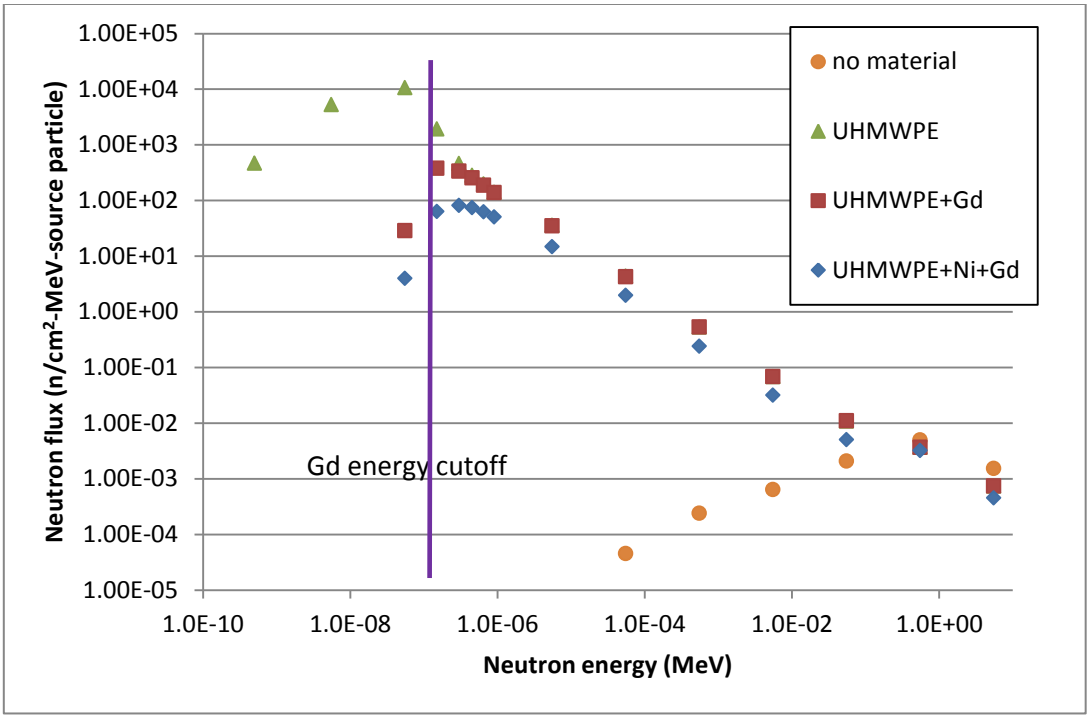

Figure 2.4. Neutron spectrum from MCNP simulations using two ^{252}Cf sources and: (1) no other material, (2) UHMWPE, (3) UHMWPE and Gd and (4) UHMWPE, Ni and Gd

The infinitely thick neutron source previously described had to be modified for the purpose of the experiment with fresh fuel. On one hand, the experimental source cannot be too thick as it needs to be stored and moved in the experiment room. On the other hand, the source cannot be too thin as the neutron flux previously simulated would be considerably lower. MCNP simulations were performed to calculate the neutron flux for different source thicknesses. The results were then compared to the neutron flux obtained with the infinitely thick neutron source. Figure 2.5 shows the reduction of the flux from the infinitely thick source for different source thicknesses. According to the results recorded in this figure, a 12-cm thick source was chosen for the experiment. This thickness guarantees a relatively convenient handling of the source pod and only a quarter of the initial neutron source flux lost.

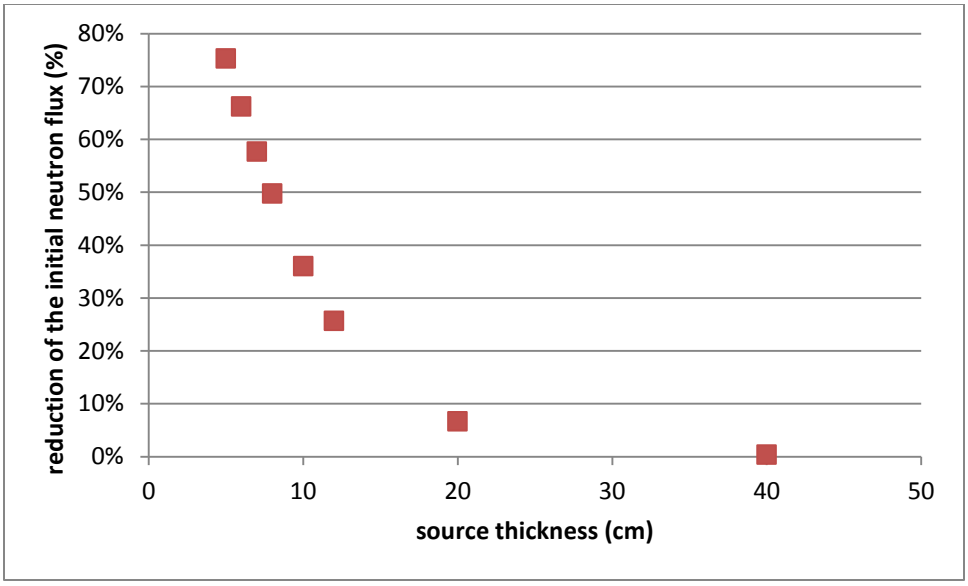

Figure 2.5. Reduction of the source neutron flux for different source thicknesses

Because of cost concerns for the validation experiment, the Gd sheet was removed from the neutron source to perform the experiment. The Gd sheet on the neutron source transmits neutrons only of energy higher than 0.13 eV and thus prevents fission events from occurring at low energy – below the Gd-Cd window. ^{239}Pu and ^{235}U have high cross sections for thermal neutrons. Thus, a thermal neutron has more chance to get absorbed than an epithermal (between 0.13 eV and 3.8 keV) or fast neutron (above 3.8 keV), which means that a thermal neutron will on average travel a shorter distance in the material than other energy neutrons. Thermal neutrons will only be interacting with the exterior part of the material as they have more chance to interact with the material before they travel to its center. As a result of series of preliminary MCNP simulations with cans of different U enrichments, it was concluded that the change in counts in each FC was fairly consistent for the different ^{235}U enrichment cans. With the Gd sheet removed from the source, the bare FC counts increase on average by 72%, the FFM counts decrease by 6%, the Gd-covered FC counts increase by 11% and the Cd-covered FC counts decrease by 3%. As the thin Gd sheet on the source cuts most thermal neutrons, it was expected to have the biggest increase in the bare FC. Gd and Cd FCs are

also influenced by the thin Gd sheet as their cutoff energies are really close to thermal energy neutrons. It is also expected that the increase in Gd FC will be higher than in Cd FC as the cutoff energy of Gd is closer to thermal energies than Cd energy cutoff. As SINRD takes into account ratios of counts, the general trend of ratios with Gd on the source will be similar as the trend of ratios without Gd, but the magnitude will be different. Consequently, as the effects of removing the thin Gd from the source have a tolerable impact on the results, the prototype of the source was built without the Gd sheet for the experiment on U cans.

2.3. Neutron Lifecycle

An analysis of the 3-group neutron lifecycle can explain the expected behavior for the instrument. The neutron source described in section 2.2, with a thin Gd sheet on the surface, emits a source of neutrons with two energy groups: fast neutrons (S_{fast}) and epithermal neutrons (S_{epi}). The thermal neutrons from the source are absorbed in the Gd filter.[8] Then, these source neutrons will either reach the material being interrogated and interact with it or leak to the FCs in the detector pod. If the source neutrons cause fission in the material, then new fast neutrons are created which can in turn interact with the material or leak to the detector.

The behavior of a neutron in a system can be described analytically by probabilities depending on the material composition and geometry of the system. The following probabilities drive neutron behavior in the system:

- P_{FNL} = fast neutron non-leakage probability = probability that a fast neutron does not leak given that it was injected into the system

[8] For simplicity, only one epithermal source term emitting neutrons of energies between the fast cutoff and the Cd cutoff has been considered in the lifecycle discussed below. To be rigorously correct, another epithermal source term emitting neutrons with energies between the Cd cutoff and Gd cutoff could be added.

- P_{ENL} = epithermal neutron non-leakage probability = probability that a neutron in the system does not leak from the system given that it slowed to epithermal energies (below 3.8 keV) without being absorbed or was injected into the system at epithermal energies
- P_{ENL_Cd} = epithermal neutron non-leakage probability before Cd cutoff = probability that a neutron in the system does not leak from the system before slowing down to Cd cutoff energy given that it slowed to epithermal energies without being absorbed or was injected into the system at epithermal energies
- P_{ENL_Gd} = epithermal neutron non-leakage probability before Gd cutoff = probability that a neutron in the system does not leak from the system before slowing down to Gd cutoff given that it slowed to Cd cutoff energy
- P_{TNL} = thermal neutron non-leakage probability = probability that a neutron in the system does not leak from the system given that it slowed to thermal energies without being absorbed
- p_{epi} = resonance escape probability to epithermal cutoff = probability that a neutron escapes the resonances (i.e., is not absorbed) and slows to epithermal cutoff energy (below 3.8 keV) given that it did not leak while fast
- p_{epi_Cd} = resonance escape probability from epithermal cutoff to Cd cutoff = probability that a neutron escapes the resonances (i.e., is not absorbed) and slows to the Cd cutoff energy (below 1.25 eV) given that it did not leak while epithermal above Cd cutoff
- p_{th} = resonance escape probability from Cd cutoff to thermal cutoff = probability that a neutron escapes the resonances (i.e., is not absorbed) and slows to thermal energies (below the Gd cutoff or 0.13 eV) given that it did not leak while epithermal nor get absorbed slowing down to Cd cutoff
- u_f = fast fissionable material utilization = probability that a neutron is absorbed in fissionable material given that it was absorbed while fast

- u_{epi} = epithermal fissionable material utilization = probability that a neutron is absorbed in fissionable material given that it was absorbed while epithermal
- u_{epi_Cd} = epithermal fissionable material utilization before Cd cutoff = probability that a neutron is absorbed in fissionable material given that it was absorbed while slowing down to Cd cutoff energy
- u_{epi_Gd} = epithermal fissionable material utilization before Gd cutoff = probability that a neutron is absorbed in fissionable material given that it was absorbed while slowing down from Cd cutoff energy to Gd cutoff energy
- f = thermal fissionable material utilization = probability that a neutron is absorbed in fissionable material given that it was absorbed while thermal
- P_{FF} = fast fission probability = probability that a neutron will cause a fission reaction given that it was absorbed in fuel while fast
- P_{EF} = epithermal fission probability = probability that a neutron will cause a fission reaction given that it was absorbed in fuel while epithermal
- P_{EF_Cd} = epithermal fission probability before Cd cutoff = probability that a neutron will cause a fission reaction given that is was absorbed in fuel while slowing down from the epithermal cutoff energy to Cd cutoff energy
- P_{EF_Gd} = epithermal fission probability before Gd cutoff = probability that a neutron will cause a fission reaction given that is was absorbed in fuel while slowing down from Cd cutoff energy to Gd cutoff energy
- P_{TF} = thermal fission probability = probability that a neutron will cause a fission reaction given that it was absorbed in fuel while thermal
- ν_f = neutrons per fast fission = expected number of fast neutrons produced per fast fission
- ν_{epi} = neutrons per epithermal fission = expected number of fast neutrons produced per epithermal fission

- ν_{epi_Cd} = neutrons per epithermal fission occurring before Cd cutoff = expected number of fast neutrons produced per epithermal fission occurring from a neutron with energy between the epithermal cutoff and the Cd cutoff
- ν_{epi_Gd} = neutrons per epithermal fission occurring between Cd and Gd cutoff = expected number of fast neutrons produced per epithermal fission occurring from a neutron of energy between the Cd cutoff and Gd cutoff
- ν_{th} = neutrons per thermal fission = expected number of fast neutrons produced per thermal fission
- ε_{FFM} = absolute efficiency of the FFM detector = probability that a neutron is counted in the FFM given that it leaked from the system while fast
- ε_{Cd} = absolute efficiency of the Cd detector = probability that a neutron is counted in the Cd covered detector given that it leaked from the system while epithermal
- ε_{Gd} = absolute efficiency of the Gd detector = probability that a neutron is counted in the Gd covered given that it leaked from the system while epithermal
- ε_{bare} = absolute efficiency of the bare detector = probability that a neutron is counted in the bare detector given that it leaked from the system while thermal

One should note that the neutron energy groups have been defined for this problem according to the different FCs used in the detector pod. Thus, the fast and epithermal groups have their lower bound respectively determined by the B_4C energy cutoff (3.8 keV) and Gd energy cutoff (0.13 eV). A subgroup has been created in the epithermal group to take into account the Cd energy cutoff (1.25 eV). In general, these probabilities are all conditional probabilities conditioned on the neutrons previous history in the system. Due to this, we also see that the following identity is true given our definitions above:

$$P_{ENL} = P_{ENL\_Cd} P_{ENL\_Gd} \tag{2.1}$$

The neutron lifecycle, illustrated by Figure 2.6, is centered on the measured material located between the neutron source on one side and the detector on the other side. Thus, the inputs in this lifecycle are neutrons coming from the source and the output are neutrons leaking to the FCs. The neutron lifecycle begins with neutrons of different energies – fast and epithermal– coming from the source and entering the material.

A fast source neutron is considered first to illustrate the neutron lifecycle. The probability that a fast source neutron does not leak to the detector is P_{FNL}, the fast non-leakage probability. If it did not leak while fast, p_{epi} is the probability that the neutron does not get absorbed in resonances while slowing down from fast to the epithermal cutoff energy (3.8 keV). The probability that this neutron does not leak from the material while in the energy range between epithermal and the Cd cutoff is P_{ENL_Cd}. If it did not leak in this energy range, then the probability that it is not absorbed in a resonance while slowing down to the Cd cutoff is p_{epi_Cd}. The probability that this neutron does not leak from the material while in the energy range between the Cd and Gd cutoff is P_{ENL_Gd}. If it did not leak while epithermal, p_{th} is the probability that the neutron is not absorbed in a resonance while slowing down from the Cd cutoff to thermal (below 0.13-eV Gd cutoff). P_{TNL} is the probability that the neutron does not leak while thermal. If it gets absorbed while thermal, f is the probability that this thermal neutron get absorbed by fissionable material given that it is absorbed. P_{TF} is the probability that thermal absorption in fissionable material causes fission. If a thermal fission occurs, v_{th} is the average number of neutrons emitted per thermal fission, and these new neutrons are born fast.

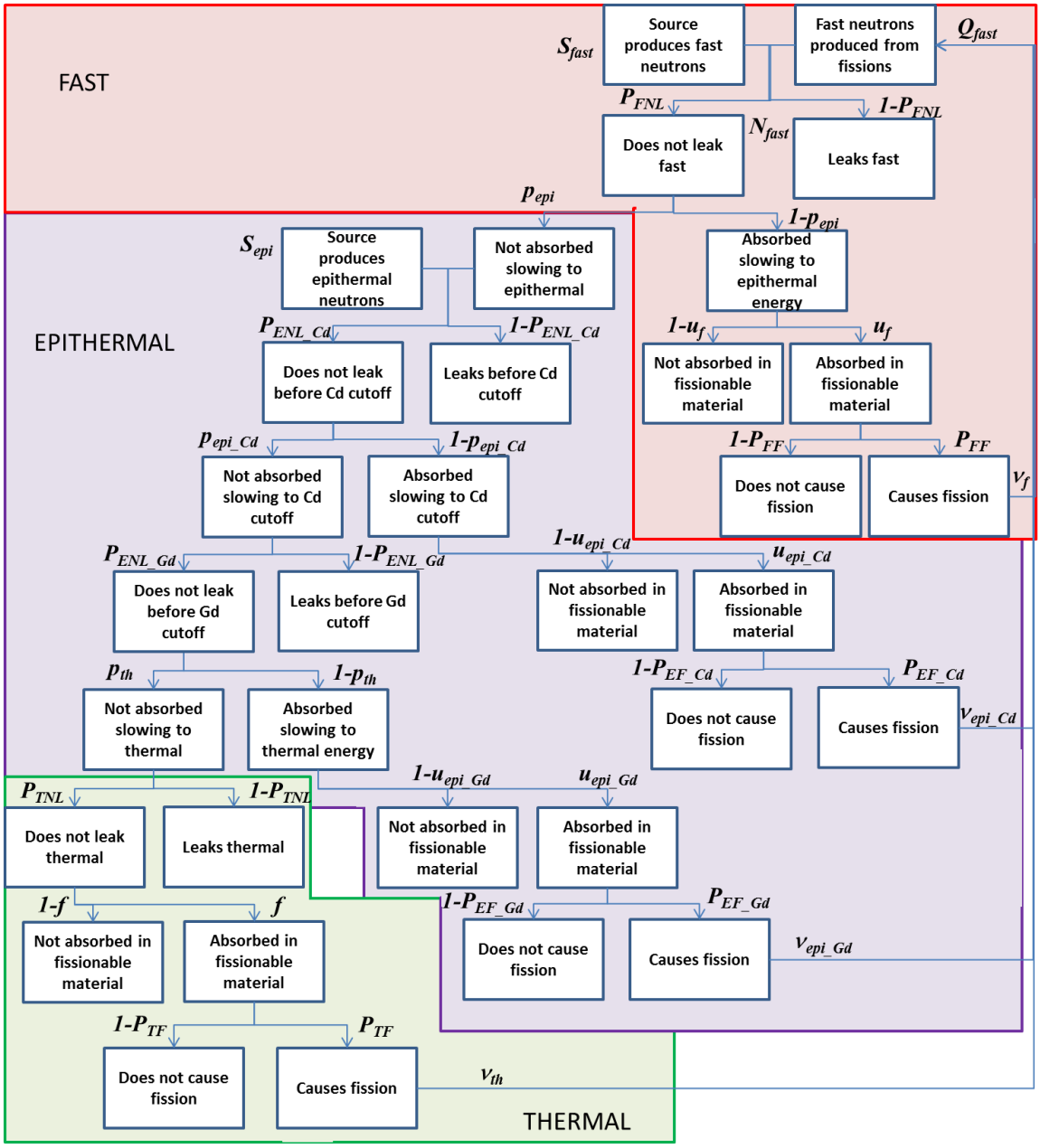

Figure 2.6. 3-group neutron lifecycle

The number of fast neutrons in the system is equal to the number of initial fast neutrons emitted by the neutron source (S_{fast}) plus a number of neutrons (Q_{fast}) depending on the fission events occurring and the average number of neutrons emitted

per fission. The number of neutrons produced by fission events in the system is given by:

$$Q_{fast} = (S_{fast} + Q_{fast})P_{FNL}(1 - p_{epi})u_f P_{FF} v_f + [(S_{fast} + Q_{fast})P_{FNL}p_{epi} + S_{epi}]P_{ENL\_Cd}\ (1 - p_{epi\_Cd}\ )u_{epi\_Cd}P_{EF\_Cd}v_{epi\_Cd} + [(S_{fast} + Q_{fast})P_{FNL}p_{epi} + S_{epi}]P_{ENL\_Cd}\ p_{epi\_Cd}P_{ENL\_Gd}\,(1 - p_{th})u_{epi\_Gd}P_{EF\_Gd}v_{epi\_Gd} + [(S_{fast} + Q_{fast})P_{FNL}p_{epi} + S_{epi}]P_{ENL\_Cd}p_{epi\_Cd}P_{ENL\_Gd}p_{th}P_{TNL}fP_{TF}v_{th} \quad (2.2)$$

If the probability of a fast neutron that was born from fission in the sample not leaking from the sample was zero, then the number of fast neutrons produced by fission events in the system is given by:

$$Q_{fast} = S_{fast}P_{FNL}(1 - p_{epi})u_f P_{FF} v_f + [S_{fast}P_{FNL}p_{epi} + S_{epi}]P_{ENL\_Cd}\ (1 - p_{epi\_Cd}\ )u_{epi\_Cd}P_{EF\_Cd}v_{epi\_Cd} + [S_{fast}P_{FNL}p_{epi} + S_{epi}]P_{ENL\_Cd}\ p_{epi\_Cd}P_{ENL\_Gd}\,(1 - p_{th})u_{epi\_Gd}P_{EF\_Gd}v_{epi\_Gd} + [S_{fast}P_{FNL}p_{epi} + S_{epi}]P_{ENL\_Cd}p_{epi\_Cd}P_{ENL\_Gd}p_{th}P_{TNL}fP_{TF}v_{th} \quad (2.3)$$

This simplifies to:

$$Q_{fast} = S_{fast}\left\{P_{FNL}(1 - p_{epi})u_f P_{FF} v_f + \left[P_{FNL}p_{epi} + \frac{S_{epi}}{S_{fast}}\right]P_{ENL\_Cd}\ (1 - p_{epi\_Cd}\ )u_{epi\_Cd}P_{EF\_Cd}v_{epi\_Cd} + \left[P_{FNL}p_{epi} + \frac{S_{epi}}{S_{fast}}\right]P_{ENL\_Cd}\ p_{epi\_Cd}P_{ENL\_Gd}\,(1 - p_{th})u_{epi\_Gd}P_{EF\_Gd}v_{epi\_Gd} + \left[P_{FNL}p_{epi} + \frac{S_{epi}}{S_{fast}}\right]P_{ENL\_Cd}p_{epi\_Cd}P_{ENL\_Gd}p_{th}P_{TNL}fP_{TF}v_{th}\right\} \quad (2.4)$$

Therefore the total number of fast neutrons inserted into the sample per cycle is given by:

$$N_{fast} = S_{fast}M \quad (2.5)$$

Where M is the sample multiplication and is well approximated by

$$M = 1 + P_{FNL}(1 - p_{epi})u_f P_{FF} v_f + \left[P_{FNL} p_{epi} + \frac{S_{epi}}{S_{fast}}\right] P_{ENL\_Cd} \left(1 - p_{epi\_Cd}\right) u_{epi\_Cd} P_{EF\_Cd} v_{epi\_Cd} + \left[P_{FNL} p_{epi} + \frac{S_{epi}}{S_{fast}}\right] P_{ENL\_Cd} \; p_{epi\_Cd} P_{ENL\_Gd} (1 - p_{th}) u_{epi\_Gd} P_{EF\_Gd} v_{epi\_Gd} + \left[P_{FNL} p_{epi} + \frac{S_{epi}}{S_{fast}}\right] P_{ENL\_Cd} p_{epi\_Cd} P_{ENL\_Gd} p_{th} P_{TNL} f P_{TF} v_{th} \quad (2.6)$$

Only the neutrons which leak from the material can contribute to the counts recorded by the detectors, but each neutron which leaks will not necessarily reach the FCs and cause a count. The absolute efficiency of the FCs (ε), which is dependent on the detector characteristics and the counting geometry, will determine the number of counts per neutron that leaks from the sample.

The FFM measures the fast neutrons from the neutron source and from fission events which leak from the material. The count rate in this FC is a function of the source strength, the neutron multiplication and the fast leakage probability. The expected count rate in the FFM is given by:

$$C_{FFM} = (S_{fast} M)(1 - P_{FNL})\varepsilon_{FFM} \quad (2.7)$$

where C_{FFM} is the count rate in the FFM in counts per second (cps).

The bare FC records the thermal neutron leakage from the measured material. If we assume that the bare FC counts are dominated by the thermal neutron leakage, then the expected count rate in bare FC is given by:

$$C_{bare} = (S_{fast}\, M P_{FNL}\, p_{epi} + S_{epi}) P_{ENL\_Cd} p_{epi\_Cd} P_{ENL\_Gd} P_{th} (1 - P_{TNL}) \varepsilon_{bare} \quad (2.8)$$

This FC primarily measures the source strength as well as the neutron multiplication, the resonance escape probability from fast to thermal energies, and the thermal leakage probability of the material.

The Gd- and Cd-covered FCs are used to form a window around the 0.3 eV resonance of ^{235}U and ^{239}Pu fission cross-sections. The count rates recorded by these FCs

are related to the resonance escape probability from fast to epithermal energies and to the epithermal leakage probability. The expected count rates in the Gd- and Cd-covered FCs (C_{Gd} and C_{Cd}, respectively) are given by:

$$C_{Gd} = \left[\left(S_{fast}M\right)P_{FNL}p_{epi} + S_{epi}\right]\left[\left(1 - P_{ENL\_Cd}\right) + P_{ENL\_Cd}p_{epi-Cd}\left(1 - P_{ENL\_Gd}\right)\right]\varepsilon_{Gd} \quad (2.9)$$

$$C_{Cd} = \left[\left(S_{fast}M\right)P_{FNL}p_{epi} + S_{epi}\right]\left(1 - P_{ENL\_Cd}\right)\varepsilon_{Cd} \quad (2.10)$$

SINRD uses ratios of counts from different FCs to reduce the sensitivity of the measurements to extraneous material present in the fissile isotope-bearing material. Depending on the material measured, the ratios that are the most sensitive to the fissile material content will be used for fissile content quantification. The uncertainties in the data will also determine the ratios to consider for this quantification. Using equations (2.7) to (2.10), several ratios are derived to illustrate the SINRD method. For instance, the bare to FFM FC ratio is acquired by dividing equation (2.8) by equation (2.7) and after some simplifications is given by:

$$\frac{C_{bare}}{C_{FFM}} = \frac{\varepsilon_{bare}}{\varepsilon_{FFM}}\left(\frac{S_{fast}MP_{FNL}p_{epi}+S_{epi}}{S_{fast}M}\right)\left[\frac{P_{ENL\_Cd}p_{epi\_Cd}P_{ENL\_Gd}P_{th}(1-P_{TNL})}{1-P_{FNL}}\right] \quad (2.11)$$

The bare/FFM ratio is proportional to the ratio of detector efficiencies [the first term in equation (2.11)] which is a constant. The second term in equation (2.11) is simply the ratio of the epithermal neutron source to the fast neutron source. The number of epithermal source neutrons relative to the number of fast neutrons entering the system ($S_{epi}/S_{fast}M$) is a characteristic of the source and makes this term essentially a constant. The total resonance escape probability formed by $p_{epi}p_{th}$, the leakage probabilities for the three energy groups and the neutron multiplication are the quantities that will change the bare/FFM ratio. These quantities are a function of the system geometry and the composition of the measured material. They are sensitive to the quantity of resonance and thermal absorbers including fissile isotopes (^{235}U, ^{239}Pu). With an increase of the fissile content in the material, more thermal neutrons will be absorbed and more fission events will occur. Consequently, counts in the bare FC are expected to decrease while counts in the FFM are expected to increase with increasing fissile content. Thus, the

bare/FFM ratio is expected to be lower for larger fissile content in the measured material.

The relationship for the (Gd-Cd) to FFM FCs ratio is derived using equations (2.9), (2.10) and (2.7). This ratio is given by:

$$\frac{C_{Gd}-C_{Cd}}{C_{FFM}} = \left(\frac{\varepsilon_{Gd}}{\varepsilon_{FFM}}\right)\left(\frac{S_{fast}MP_{FNL}p_{epi}+S_{epi}}{S_{fast}M}\right)\left(\frac{1-P_{ENL\_Cd}}{1-P_{FNL}}\right)\left[1-\frac{\varepsilon_{Cd}}{\varepsilon_{Gd}}+ p_{epi-Cd}P_{ENL\_Cd}\frac{1-P_{ENL\_Gd}}{1-P_{ENL\_Cd}}\right] \quad (2.12)$$

The first term in this ratio is simply the ratio of the efficiencies between the Gd-covered FC and the FFM which is a constant. The second term is again the ratio of the epithermal neutron source to the fast neutron source which is also essentially a constant. The third term is the ratio of the epithermal leakage probability before Cd cutoff to the fast leakage probability which would be a constant for samples of similar geometry. Similar to the bare to FFM ratio, the (Gd-Cd)/FFM ratio depends on the constants $S_{epi}/S_{fast}M$. The ratio will be sensitive to the resonance escape probability for a neutron to escape resonances between the Cd and Gd cutoffs ($1 - P_{ENL\_Gd}$). Contrary to the Cd-covered FC, the counts recorded by the Gd-covered FC are sensitive to the amount of absorbers having resonances between 0.13 eV and 1.25 eV – for example ^{239}Pu with its large 0.3 eV resonance. Thus, the (Gd-Cd)/FFM ratio is mostly sensitive to absorbers that have resonances within this energy window. With increasing of fissile content that has resonances in the (Gd-Cd) energy window, the counts recorded in the window are expected to decrease due to neutron absorption in the resonances. In addition, the number of fission events is expected to increase with the fissile content. Consequently, it is expected that the (Gd-Cd)/FFM ratio be lower for higher fissile content.

The Gd to FFM ratio is given by the following relationship:

$$\frac{C_{Gd}}{C_{FFM}} = \frac{\varepsilon_{Gd}}{\varepsilon_{FFM}}\left(\frac{\left(1-P_{ENL_{Cd}}\right)+P_{ENL_{Cd}}P_{epi_{Cd}}(1-P_{ENL_{Gd}})}{1-P_{FNL}}\right)\left(P_{FNL}p_{epi}+\frac{S_{epi}}{S_{fast}M}\right) \quad (2.13)$$

As with previous ratios, the relative detector efficiencies, the epithermal leakage to fast leakage relationship, and the ratio of source neutrons are constants. The Gd to FFM ratio is primarily influenced by the resonance escape probability from epithermal to Gd cutoff and will depend on the quantity of absorbers in the measured material that have resonances above the Gd cutoff energy. With increasing of fissile content, the counts recorded in the Gd FC are expected to decrease due to neutron absorption in epithermal resonances. In addition, the number of fission events is expected to increase with the fissile content. Consequently, it is expected that the Gd/FFM ratio be lower for higher fissile content.

The Gd to Cd ratio is given by

$$\frac{C_{Gd}}{C_{Cd}} = \frac{\varepsilon_{Gd}}{\varepsilon_{Cd}} \left(1 + \frac{P_{ENL_{Cd}}}{1 - P_{ENL_{Cd}}} P_{epi_{Cd}} (1 - P_{ENL_{Gd}}) \right. \tag{2.14}$$

This is the simplest of the ratios since it essentially only depends on the change in the resonance escape probability from the Cd to Gd cutoff energies. As the quantity of absorber in this region increases (due to increased ^{239}Pu or ^{235}U content), then this ratio is expected to increase proportionally to this change.

2.4. Features Used in MCNP Simulations

The simulations performed during this research have been performed using MCNP. MCNP is a numerical tool largely used for nuclear engineering applications. It uses the Monte Carlo method to track particles from birth to death. MCNP generates random numbers which are used to determine the distance a particle will travel or which interaction will occur [26]. The advantages that MCNP presents over a deterministic code are: (1) the simulation uses detailed physics and can simulate very complex geometries, (2) the sampling is continuous for energy and angle, (3) the MCNP solution is given only at the locations the user requests, and (4) a statistical error is associated with the solution. An example of input file is included in Appendix B.

2.4.1. MCNP tallies

A tally in MCNP specifies which physical value to be calculated by the code. This research uses the neutron flux averaged over a surface (F2 tally) and the neutron flux averaged over a cell (F4 tally), both in units of neutrons/cm^2. The F2 tally has been used to determine the neutron spectrum emerging from the neutron source. It was used along with an energy binning card (e2 card) to record the neutron spectrum for several energy bins separately. As the computational time increases with the number of energy bins, it is important to choose relevant bins. Each tally calculated is normalized by the number of source particles run for the simulation. In addition, a relative error is associated with each tally result. The internal MCNP statistical checks on the tally are used to evaluate the quality of a simulation. For instance, the relative error of the F2 or F4 tally should be less than 5% to be considered statistically acceptable [26].

The F4 tally can also be modified with an FM4 card to get a reaction rate in units of reactions/cm^3 [26]. This modified F4 card has been used to calculate the fission rate in the FCs and the (n,p) reaction rate in the ^{3}He tubes. It has been assumed that each reaction occurring in the detector gives a count. To be able to compare a reaction rate from an MCNP simulation to a count rate experimentally recorded, the calculated reaction rate has to be normalized by the source strength used experimentally (in units of n/s).

2.4.2. MCNP source definitions

In the instrument designed, two ^{252}Cf sources supply neutrons. These two sources are modeled as point sources in MCNP. The sources are defined with an SDEF card specifying the position of the sources and their energy distribution. The watt fission spectrum for ^{252}Cf MCNP feature was used to create the neutron energy spectrum emitted from spontaneous fission of ^{252}Cf. As a default in MCNP, the two sources are considered isotropic [26].

To reduce the total computational time required, a surface source write (SSW) card has been used. The SSW capability of MCNP allows the user to record the particles

that cross a defined surface with their position, direction and energy [26]. For the simulations performed for this research, a SSW has been created at the front face of the source pod. Thus, for simulations with the material and the detector, the recorded surface source replaces the modeled source. This effectively allows for dividing the simulation into two simulations: one to transport the neutrons from the ^{252}Cf sources to the front surface of the source pod and then a second simulation to transport the neutrons from the front surface of the source pod to the detectors. This technique has the advantage of allowing resampling for changes in the detector pod to be made without needing to repeat the source calculation.

2.4.3. S(α,β) feature

The scattering law S(α,β) is essential to get a correct answer in problems involving neutron thermalization with molecules and crystalline solids [26]. For this type of materials, it is considered that neutrons of energies less than 4 eV interact with the entire molecule and not with the elements of the molecule separately. An MT card is used in MCNP to reflect this scattering of low energy neutrons in the model. This scattering law is used for UHMWPE. Figure 2.7 shows the effect of this scattering law in MCNP. This figure has been generated with MCNP Visual Editor and shows fast neutrons in red and thermal neutrons in blue. The two dense red areas correspond to the location of the two ^{252}Cf source where mostly fast neutrons are born. The scattering law in UHMWPE considerably increases the number of thermal neutrons that we can see in the neutron source.

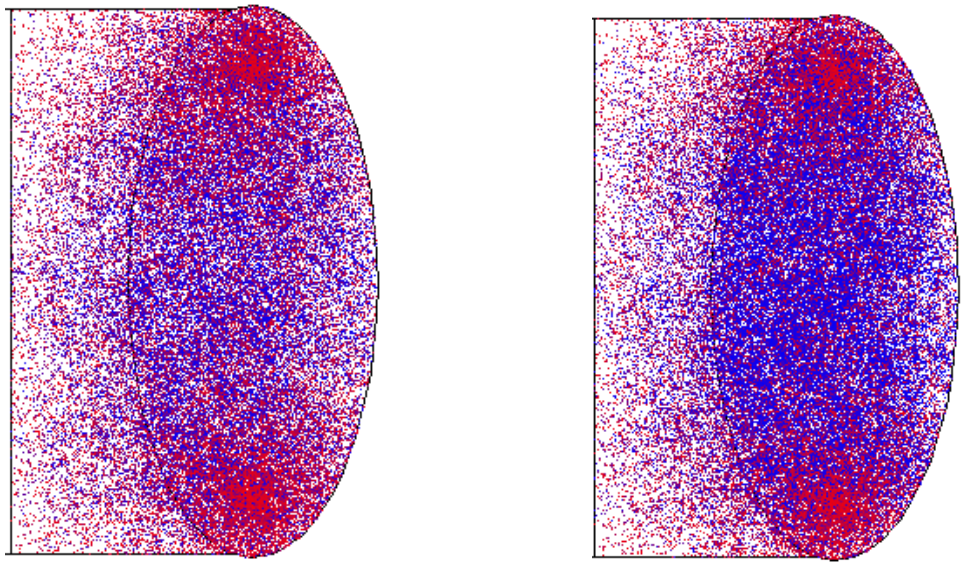

(a) (b)

Figure 2.7. Neutrons generated by the neutron source (a) without and (b) with MCNP scattering law in UHMWPE

3. VALIDATION OF THE INSTRUMENT AND MODEL WITH FRESH FUEL

To validate the MCNP model of the instrumentation, experiments have been conducted using prototypes of the source system and SINRD detector pod. First, the source system alone, and then the detector pod with the source system were tested. Based on the configuration used in the experiment, MCNP simulations using the same geometric setup as the experiment were performed. The results obtained from the simulations were compared to the experimental ones.

3.1. Validation of the Source Model

3.1.1. Experimental procedure

Bare, Gd-covered and Cd-covered detectors were used to record count rates for different neutron energy ranges. The bare detector records counts from thermal neutrons (below 0.13 eV). Gd and Cd-covered detector records counts from epithermal neutrons (above 0.13 eV for Gd and 1.25 eV for Cd). Because of their high efficiency, ^{3}He tubes have been chosen to perform this validation. According to preliminary MCNP simulations, it was determined that a 12-hour counting time would give uncertainties in counts less than 0.06%. These uncertainties were considered low enough to be able to validate the source system model. The following experimental procedure was used:

1) Measure at the same time the response of a bare, Gd-covered and Cd-covered ^{3}He tubes to background radiation during 30 minutes.
2) Setup the three detectors in front of the source system and measure their response for 12 hours.

Figure 3.1 shows the experimental setup of the detectors with the source system (a) and the corresponding model (b). The centers of the detectors were aligned in front of the face of the source system at 3.75 cm. The Cd and Gd detectors centers were respectively 3.14-cm and 2.98-cm distant from the bare detector. The geometric setup was chosen in order to maximize the solid angle from which the detectors see the source

system. The closer the detectors are from the front of the source, the larger the solid angle and the larger the number of neutrons entering the detectors. The material constraints were also considered to determine the geometric setup. The ^{3}He tubes were all of the same type (see section 2.1).

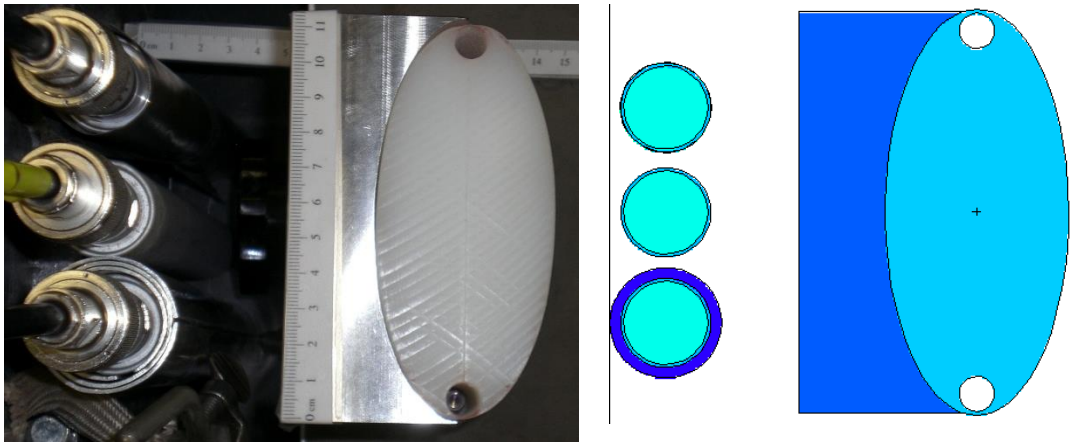

(a) (b)

Figure 3.1. Setup to validate the model of the source: (a) experimental setup, and (b) model of the experimental setup

3.1.2. Comparison between MCNP and experimental detector response

Figure 3.2[9] shows the count rates recorded by the detectors during the experiment as well as the count rates calculated using MCNP. Since the Gd and Cd filter absorbs a part of the thermal neutrons detected by the bare detector, it is expected to observe count rates lower from Gd and Cd-covered detectors compared to the bare detector, and higher from Gd compared to Cd-covered detector.

The comparison between calculated and measured ^{3}He tubes response to the source shows a higher count rate recorded in the experiment compared to the simulation.

[9] On this figure, the error bars are too small to be visualized.

This may be due to neutrons reflected back into the system from shielding, the walls of the room, the table where the material was set up, and other extraneous materials. None of these details were modeled in the MCNP simulation. The MCNP to experiment count rates ratios for bare, Gd and Cd detectors are respectively 0.858 ± 0.003, 0.911 ± 0.003, and 0.922 ± 0.003. These results demonstrate a good agreement between the calculated and measured count rates and it was determined that the MCNP source system sufficiently accurately models the physics of the experiment.

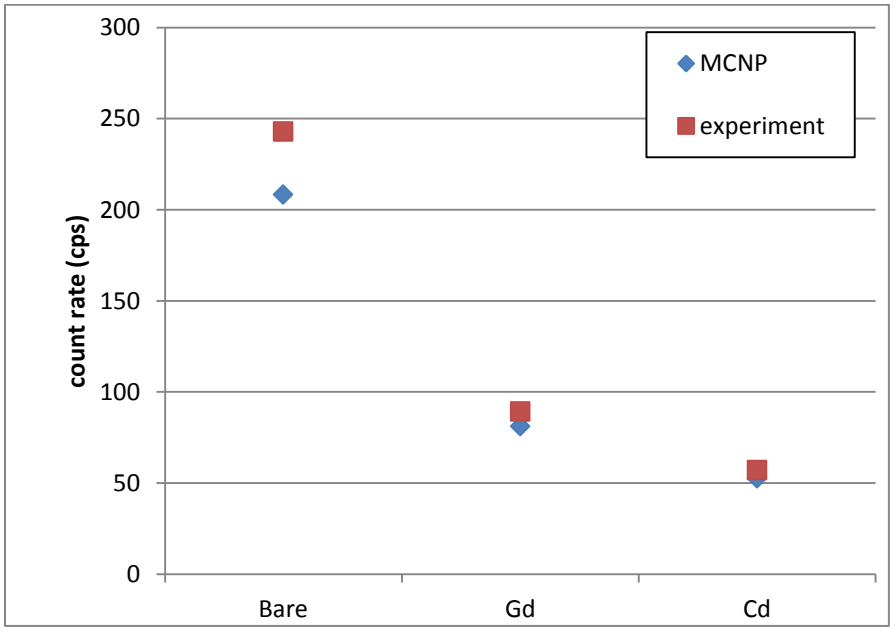

Figure 3.2. Count rates measured and calculated at the front face of the source system

3.2. Validation of the Detector Model

3.2.1. Instrumentation setup

To validate the MCNP model of the complete instrument (detector pod and source pod), a comparison between MCNP simulations and experiments both using fresh

fuel were performed. Cans with U of different enrichments (0.31 wt%, 0.71 wt%, 1.94 wt%, 2.95 wt%, and 4.46 wt%) were assayed. An empty can was also available for normalization purposes. The different enrichment as well as the dimensions and the materials used for the U can models and experiment follow standard Reference Materials EC-NRM-171/NBS-SRM-969 [42, 43]. These U can standards contain 200.1 g of U_3O_8 powder pressed in a 7.0 cm-diameter cylinder of height 1.5 cm (2 cm for 4.46% enriched U can). The density of U_3O_8 in the can is 2.60 g/cm^3 (3.47 g/cm^3 for 4.46% enriched U can) [42].

The can is made from ASTM 6061-T6 aluminum alloy containing impurities like silicon (Si), magnesium (Mg), iron (Fe) and copper (Cu). The top part of the can contains ultrasonic sensors and a plug for safeguards purposes. Each sample can has a unique ultrasonic spectrum [42]. This top part of the can was not modeled in MCNP and has been left as void in the model. The metallic components of the ultrasonic sensors have negligible effects on the neutron flux. Figure 3.3 shows a picture of the U can standard (a) and its MCNP model (b).

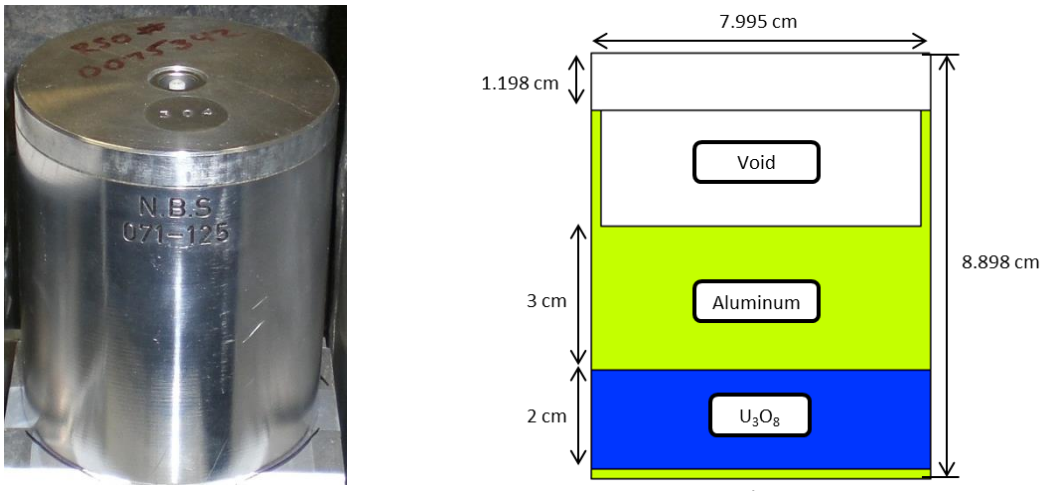

(a) (b)

Figure 3.3. U can standard: (a) picture of the can and (b) MCNP model of the can

To optimize the number of neutrons that leave the source and react with the material as well as the number of neutrons that enter the detector pod, the neutron source and the detector pod have to be placed as close as possible to the measured material. For the measurements, the U can is located at 0.7 cm from the detector pod and the source pod. Either FCs or ^{3}He tubes[10] were used in the detector pod. The center of the FCs and ^{3}He tubes is aligned with the center of the U part of the can and with the center of the neutron source pod. Figure 3.4 shows the three components in the experiment setup (a) and the corresponding MCNP model (b).

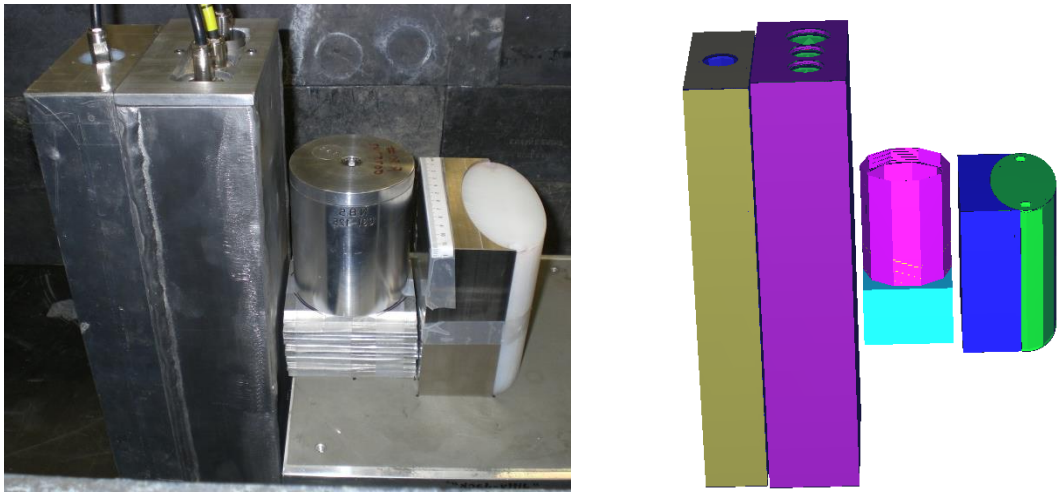

(a) (b)

Figure 3.4. Instrumentation setup: (a) experimental setup and (b) corresponding model

[10] The high efficiency of ^{3}He tubes compensates the absence of fissile material (^{235}U) in the SINRD detector pod.

3.2.2. Experimental procedure

The estimate of the measurement counting time is an important part of the experiment preparation. It is not desired that the counting time be too long because all the measurements have to be performed in a feasible time. At the same time, the counting time should not be too short because of large uncertainties concerns. It has been decided that the uncertainty of counts should be at most 3%.

The fewest counts obtained during preliminary MCNP simulations have been used to estimate the counting time needed to perform experimental measurements. The fewest counts (2.18951e-8 fissions/source particle) have been recorded by the bare FC when measurement of the 4.46 wt% ^{235}U can was simulated. Assuming 2.95e+05 n/s are emitted by each ^{252}Cf source, a 24-hour counting time is needed to get an uncertainty less or equal to 3% for each FC and for every can interrogated. The uncertainty in the counts recorded is estimated by the square root of the counts.

The experimental procedure using bare, FFM, Cd-covered, and Gd-covered detectors is the following:

1) Setup detectors (FCs and ^{3}He tubes) and verify the response to make sure all pieces of equipment perform as expected.
2) Put the FCs in SINRD instrument and record counts for 24 hours successively without any material, with the empty aluminum can, with the 0.31 wt%, 0.71 wt%, 1.94 wt%, 2.95 wt% and 4.46 wt% ^{235}U uranium cans.
3) Repeat step 3 replacing FCs by ^{3}He tubes.

The Canberra Lynx Digital Signal Analyzer [44] coupled with the Genie-2000 software [45] was used to record counts from the detectors. Each FC (or ^{3}He tube) was connected to the Lynx via a pre-amplifier; the same type of electronics was used for each detector. However, the electronic noise due to the cables used and the electronics themselves can be different for each detector. Getting the neutron spectrum from each detector, the gain and the low energy noise were adjusted independently for each detector according to the theoretical shapes of ^{3}He tube and FC spectra [46]. To make

sure that the geometry of the material setup stays the same for each measurement, markers have been placed on the experiment table.

3.2.3. Comparison of experimental measurements to MCNP results

Figure 3.5. shows the calculated and experimental count rates from ^{3}He tubes placed in the SINRD detector pod[11]. For the bare, FFM, Gd and Cd detectors, the percentage difference between MCNP and measurements are respectively 46% ± 1%, 24% ± 1%, 31% ± 1% and 12% ± 1%. The Cd detector shows the closest agreement between simulation and experiment whereas the bare detector shows the biggest difference in count rates. However, the count rates trend is comparable for calculated and measured data for each detector. Analyzing the bare and FFM count rates from simulation and experiment, it is possible to conclude that the simulations contain more thermal neutrons and the experiment more fast neutrons.

The difference between experimental measurements and MCNP results can first be attributed to the Cf sources: the location, geometry, energy spectrum and distribution of the sources are causes of bias. The simulation also does not account for any electronics error. In addition, bias concerning the detectors can occur with the location of the detector within the SINRD pod and the efficiency of the detectors. The actual thickness of the Gd and Cd filter, the presence of extraneous material and the room returning neutrons also introduced differences between simulation and experimental results. Finally, the machining of the materials for the experiment has certain tolerances that introduce bias in measurement as well.

[11] Because of equipment issues, the experimental results with FCs were inconclusive and are thus not discussed. However, MCNP results using FCs show a usable SINRD signature that could be compared to experimental results.

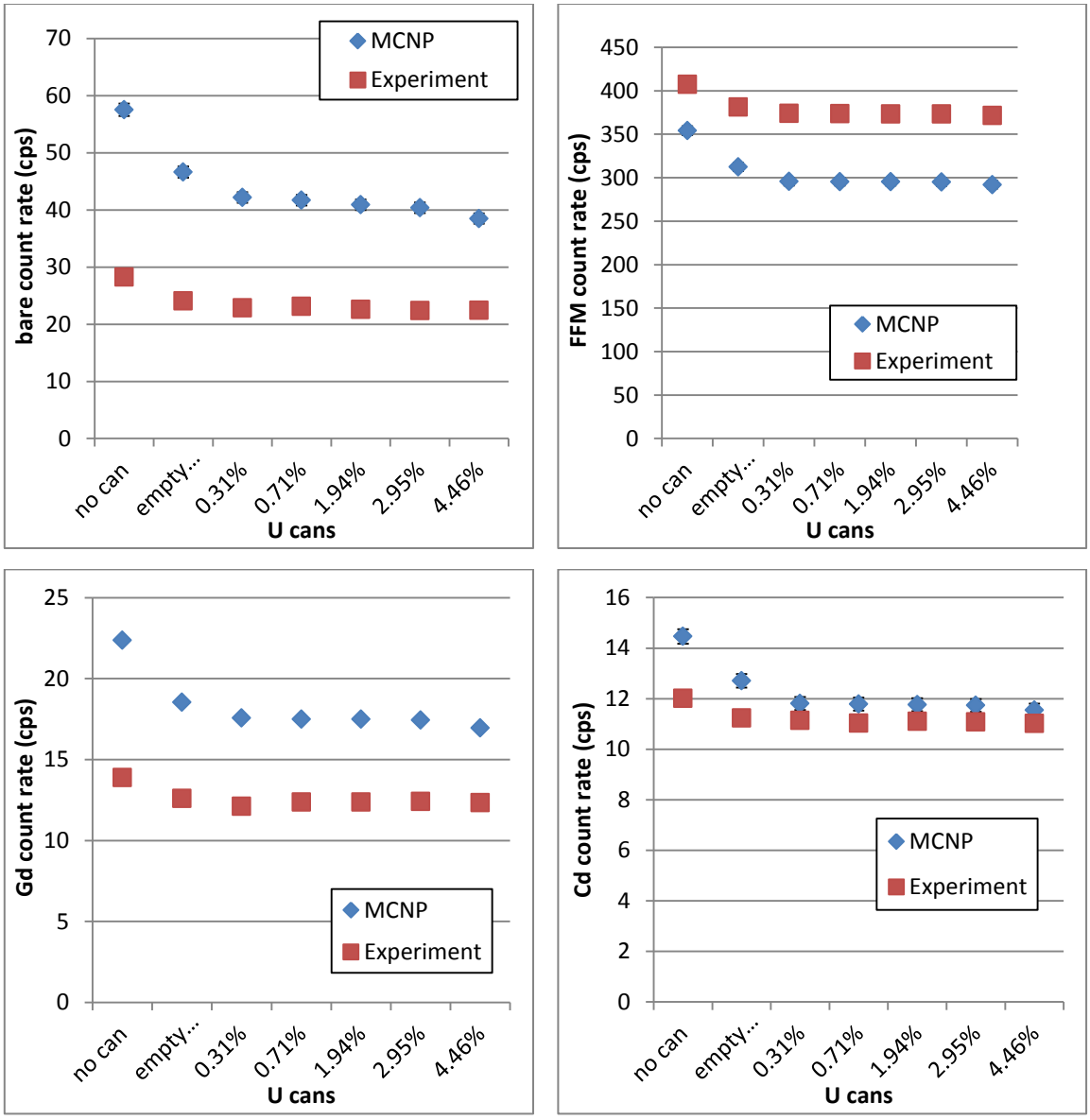

Figure 3.5. MCNP and Experimental count rates for different U can enrichment with bare, FFM, Gd and Cd ^{3}He tubes

To cancel bias in the simulations and experiment, both results have been normalized to the empty can data. The calculated to experimental (C/E) ratios have then been calculated for each SINRD ratio and for each detector, with and without

normalization. In the case where the MCNP simulations exactly model the experiment, the C/E ratio would be equal to one for each SINRD ratio and each can measured.

Figure 3.6 shows the calculated to experimental results for SINRD ratios without and with normalization to empty can SINRD ratios. The C/E ratios plotted without normalization to empty can (upper plot of the figure) shows different multiplying factors for the different SINRD ratios: the C/E ratios appear to be between 0.5 and 6. However, the normalization to the empty can case (bottom plot of the figure) brings all the C/E ratios close to one: C/E ratios range is reduced to 0.75 and 1.35. Thus, the normalization of ratios to the empty can case is necessary to get the simulations and the measurements in agreement: the MCNP model of SINRD accurately simulates the physics of the experiment.

3.2.4. SINRD response to different ^{235}U content

From the four count rates recorded by the bare, Gd, Cd, and B_4C FCs, different ratios can be calculated to analyze SINRD response. It is desirable to use ratios which show a trend as a function of fissile content with relatively low uncertainties. For the case of U cans, the normalized bare to FFM as well as the Gd to bare ratios provide the best SINRD signatures. These two ratios versus ^{235}U content are shown on Figure 3.7. Simulations with more particles will decrease the error bar of each data point and give a more precise trend for these ratios.

When measuring an unknown can, having two ratios to analyze present the advantage to compare the estimated mass of ^{235}U from each ratio separately and to then compare the results; this comparison can be useful to confirm the estimate and/or reduce the uncertainty of the estimate.

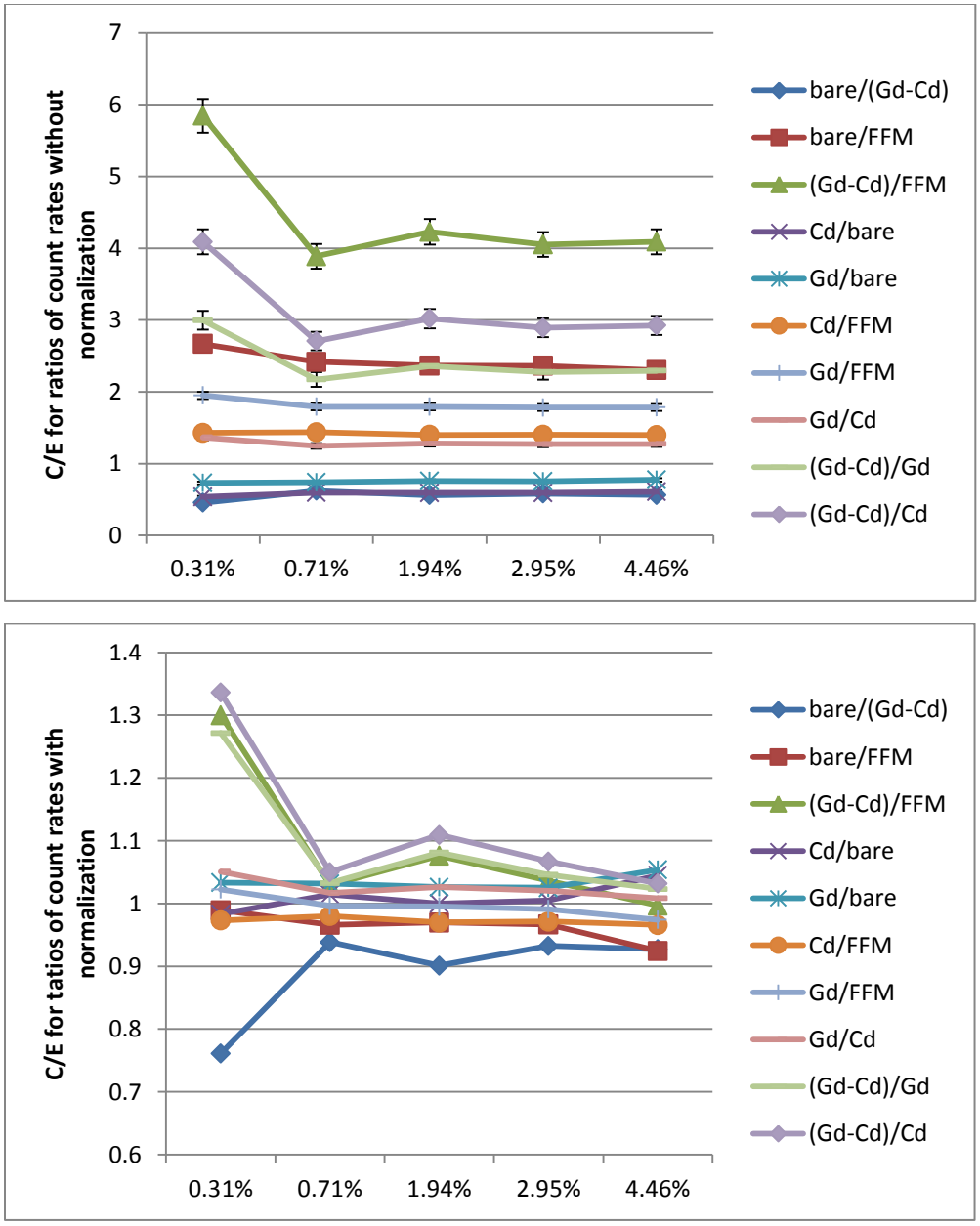

Figure 3.6. Calculated to experimental results for ratios of count rates without normalization (upper plot) and with normalization (bottom plot)

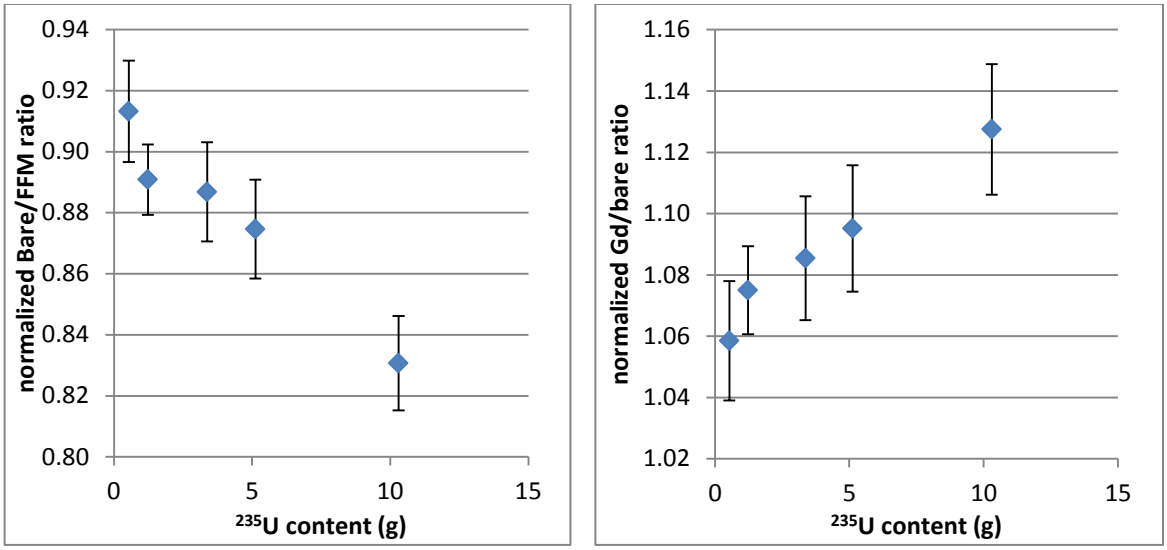

(a) (b)

Figure 3.7. Normalized bare/FFM and Gd/bare ratios versus ^{235}U content

4. ANALYSIS OF ^{239}PU-BEARING MATERIALS

The comparison between simulation and experiment results from irradiation of U cans (section 3) has shown that the MCNP model of the source and SINRD is accurately simulating the physics. The previous section has also shown that the instrument is able to quantify the ^{235}U content of fresh fuel. As ^{239}Pu is the fissile isotope of interest in pyroprocessing materials, preliminary simulations on ^{239}Pu-bearing materials have been performed: the analysis of an artificial Pu cylinder was performed to evaluate the ability of the instrument to quantify ^{239}Pu content in a material; then, calculations on a Cd-ingot were performed to analyze a pyroprocessing material.

4.1. Preliminary Analysis on a Pu Cylinder

4.1.1. Material measured

First, the instrument was tested on an artificial Pu cylinder – i.e. this material does not correspond to any pyroprocessing materials. Pyroprocessing materials are heterogeneous which motivated the use of two different densities of Pu in the cylinder. As Pu metal has a density of 19.8 g/cm^3, the densities to use had to be less than Pu metal: 16 g/cm^3 and 8 g/cm^3 were chosen. The Pu cylinder was composed of a 1-cm radius inner cylinder with a density of 16 g/cm^3 and by an outer cylinder with a radius three times bigger and a density of 8 g/cm^3. This cylinder represents approximately 2.6 kg of Pu which is less than the 10.5-kg Pu critical mass.

The Pu cylinder contains the following isotopes: ^{238}Pu, ^{239}Pu, ^{240}Pu, ^{241}Pu, and ^{242}Pu, which are the typical Pu isotopes found in spent fuel. The inner and outer cylinders have been chosen with the same Pu isotopic composition and differ only by their density. Using Oak Ridge Isotope Generation (ORIGEN2) [47] code, the Pu isotopic composition of spent fuel from the irradiation of 1.0 MT of natural U fuel in a Canada Deuterium Uranium (CANDU) reactor to a burnup of 4500 MWd/MTU at a specific power of 15.0 W/g was subjectively taken as a basis for the Pu cylinder. For

varying ^{239}Pu enrichments (between 0 and 80 at%) with the ^{240}Pu content accounting for the remainder, MCNP simulations of the instrument with Pu cylinders were performed. Table 4.1 lists the different Pu isotopic composition used for the Pu cylinder to test the instrument.

Table 4.1. Pu cylinder isotopic compositon with different ^{239}Pu content used to test the instrument

Composition #	Pu isotope content (at%)				
	^{238}Pu	**^{239}Pu**	^{240}Pu	^{241}Pu	^{242}Pu
1	0.079%	**80.004%**	10.661%	8.363%	0.893%
2	0.079%	**75.610%**	15.055%	8.363%	0.893%
3	0.079%	**65.998%**	24.667%	8.363%	0.893%
4	0.079%	**50.610%**	40.055%	8.363%	0.893%
5	0.079%	**35.611%**	55.054%	8.363%	0.893%
6	0.079%	**12.611%**	78.054%	8.363%	0.893%
7	0.079%	**3.611%**	87.054%	8.363%	0.893%
8	0.079%	**0.000%**	90.665%	8.363%	0.893%

4.1.2. Use of hafnium

In previous research on SINRD [18], the use of an Hf filter added to the Gd-covered FC has been proven to increase the detector signature for ^{239}Pu quantification. In fact, Hf absorbs neutrons of energy around 1 eV. This energy corresponds to a resonance in the ^{240}Pu total cross section. Without Hf, the neutrons being absorbed by ^{240}Pu will reduce the number of fissions occurring in the detector in the Gd-Cd energy cutoff window. A low count rate recorded in this energy window would be interpreted as a large amount of ^{239}Pu whereas ^{240}Pu absorption would actually be the cause. Figure 4.1 shows the 0.3 eV resonance of ^{239}Pu fission cross section, the 1 eV resonance of Hf and ^{240}Pu total cross section. Gd-covered FC is the only FC detecting 1 eV neutrons and is thus the only one affected by the addition of Hf.

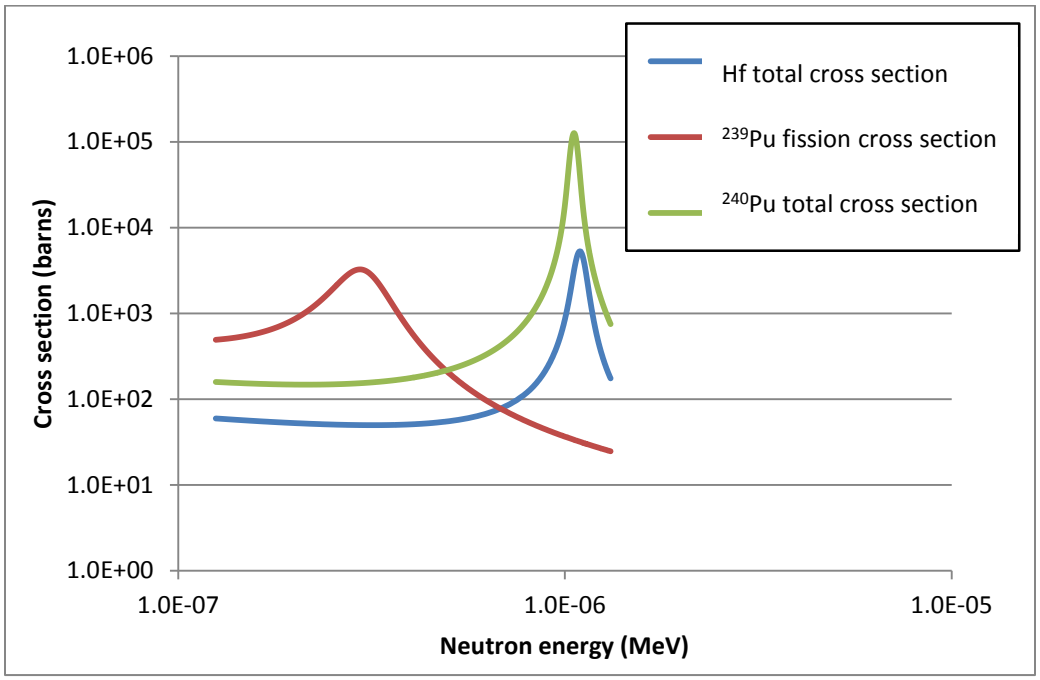

Figure 4.1. ^{239}Pu fission cross section and ^{240}Pu and Hf total cross section

To determine how much Hf is needed to absorb neutron of energies corresponding to the 1-eV resonance in ^{240}Pu total cross section, MCNP simulations have been performed on one Pu cylinder. The Pu isotopic composition #2 from Table 4.1 was chosen for the material. The neutron fluxes from the Pu cylinder through 1-mm, 2-mm and 3-mm Hf plates were compared to the neutron flux recorded without any Hf plate. Only the influence of Hf in the energy bin containing the ^{240}Pu resonance (0.8 eV – 1.2 eV) was investigated by comparing neutron fluxes. The geometry used for these simulations is shown on Figure 4.2. To cancel the effect of the ^{240}Pu resonance, the Hf thickness which decreases the neutron flux the most in the energy window 0.8 eV-1.2 eV is the optimal thickness.

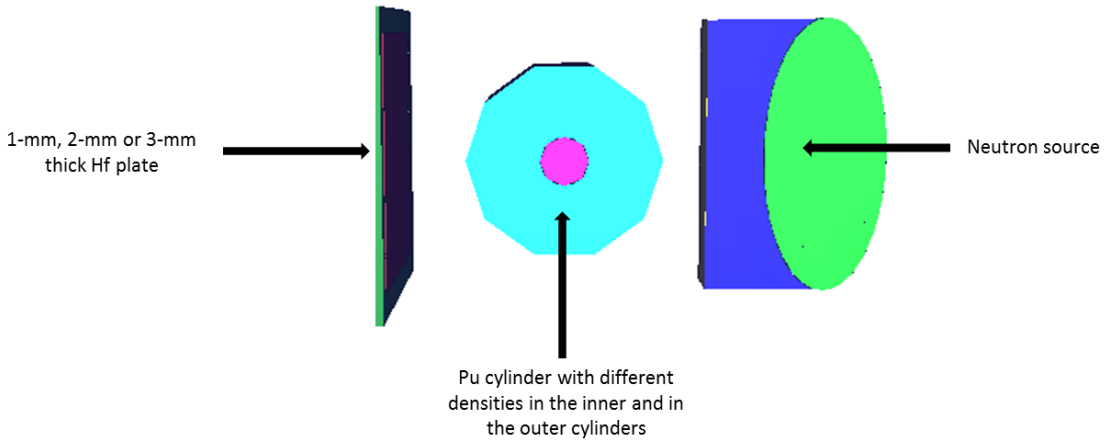

Figure 4.2. MCNP simulation to investigate the optimal Hf thickness

Table 4.2 shows the percentage of reduction of the neutron flux induced by the addition of 1-mm, 2-mm and 3-mm thick Hf plates. Only the neutron flux in the energy window 0.8 eV -1.2 eV has been analyzed in these simulations. The 3-mm thick Hf reduces the neutron flux the most in the ^{240}Pu 1-eV resonance thus, 3-mm thick Hf should be used to cancel the ^{240}Pu resonance effect on the detector signature. However, the difference between adding 2-mm thick Hf and 3-mm thick Hf is relatively small. For cost concerns, 2-mm Hf has been stated as enough to cancel the effect of ^{240}Pu to quantify ^{239}Pu in a material. In the following, all simulations have been performed wrapping the Gd-covered FC in 2-mm thick Hf.

Table 4.2. Reduction of original flux for different Hf thicknesses

Hf thickness (mm)	1	2	3
Reduction of original flux (%)	71.24	89.19	95.33

4.1.3. SINRD response to different ^{239}Pu content

The different isotopic compositions of the Pu cylinder developed in section 4.1.1 were simulated in MCNP to evaluate the ability of instrument to quantify ^{239}Pu; the geometry of the simulation is shown on Figure 4.3. Fission rates from the bare, Gd-covered, Cd-covered, and FFM detectors were recorded and ratios of these count rates were then calculated to evaluate the SINRD response. The fission rates obtained measuring the Pu cylinder without ^{239}Pu (composition #8 from Table 4.1) were used for normalization purposes. The best SINRD signature has been recorded by the normalized bare/FFM and Gd/bare ratios from U and Pu FCs.

Figure 4.4 shows these two ratios for SINRD configuration with U FCs only and U and Pu FCs. The bare/FFM ratio shows the same signature for both configurations as they both use the same type of FCs; however, the Gd/bare ratio shows a slope twice as big for U and Pu FCs compared to U FCs only. Thus, the best SINRD signature is obtained from the instrument using U and Pu FCs. The normalized FFM count rate could also be used in addition of the bare/FFM and Gd/bare ratio to confirm the estimate of ^{239}Pu content in the material. Comparing different estimates from different trends could also decrease the uncertainty of the estimate.

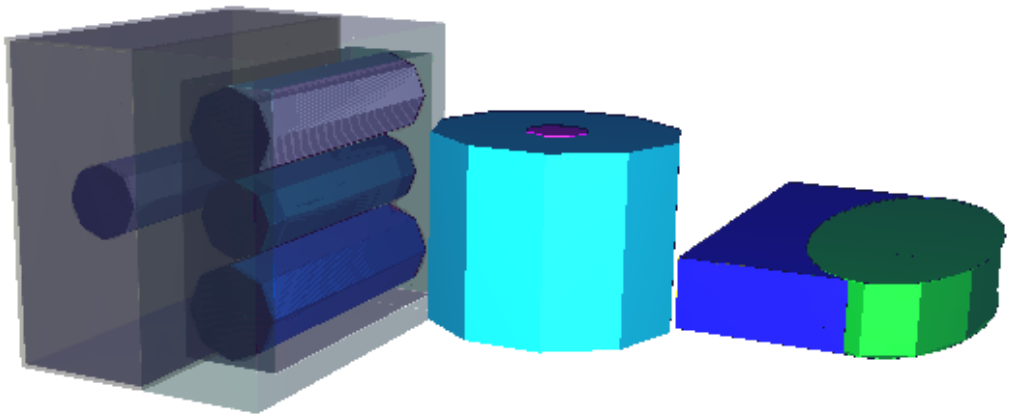

Figure 4.3. Geometry of MCNP simulations with Pu cylinder

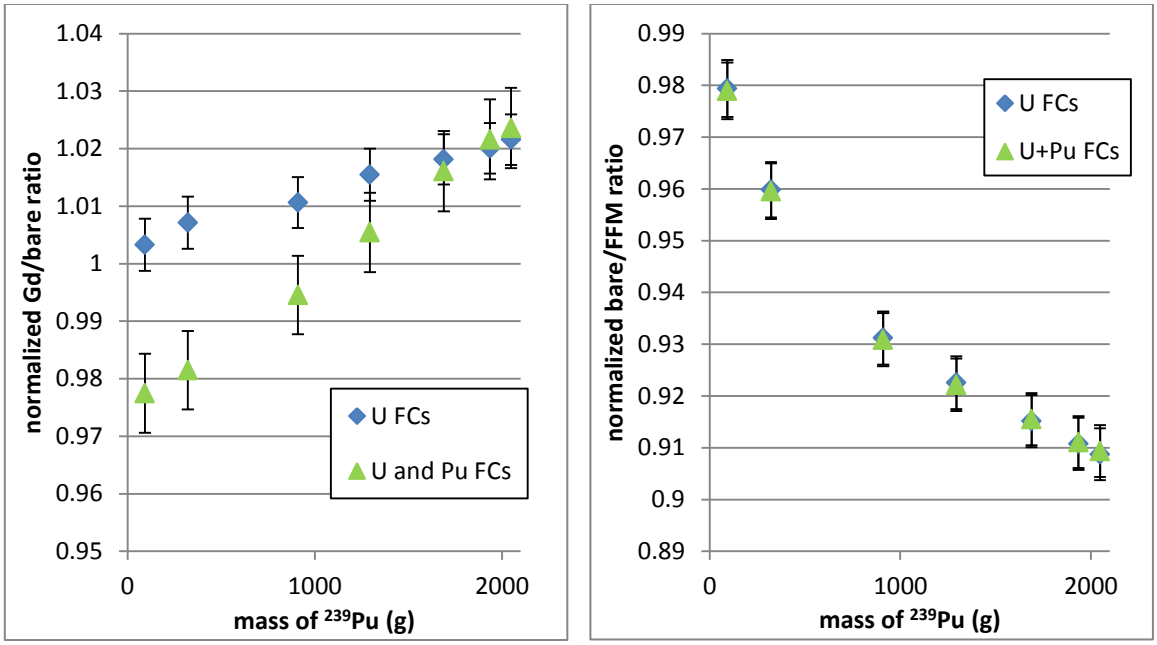

(a) (b)

Figure 4.4. Normalized Gd/bare (a) and bare/FFM (b) ratios versus 239Pu content for SINRD using U FCs only and U and Pu FCs

A test simulation has been run in MCNP to evaluate the precision of the 239Pu content estimate from the normalized bare/FFM and Gd/bare ratios, and normalized FFM count rate. A Pu cylinder containing 638.6 g of 239Pu has been simulated with the instrument. The SINRD ratios and count rates for this sample supposed unknown have been analyzed.

Figure 4.5 shows the data from this unknown plotted on the normalized bare/FFM, Gd/bare or normalized FFM count rate trends obtained from previous simulations. On the figure, the data from the unknown has been represented by a plain red horizontal line; the dash lines represent the uncertainty associated with each data. To estimate the ^{239}Pu content of the sample, the smallest and highest masses corresponding to data with uncertainty of the unknown have been calculated; the average of these two masses gives the estimate of the ^{239}Pu content and the difference between the masses and this average gives the uncertainty of the estimate.

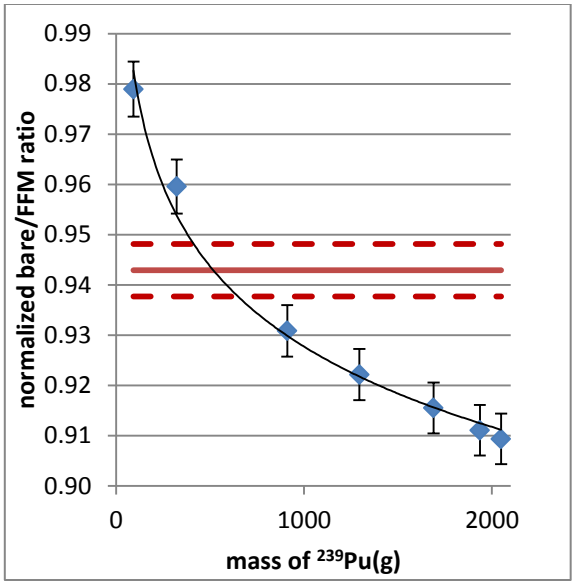

(a)

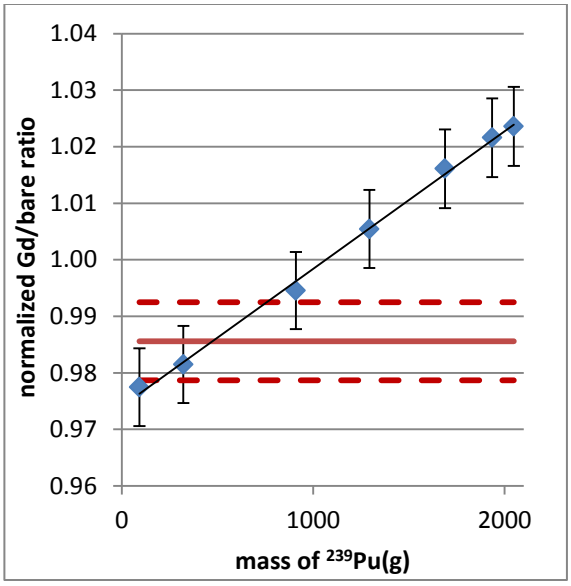

(b)

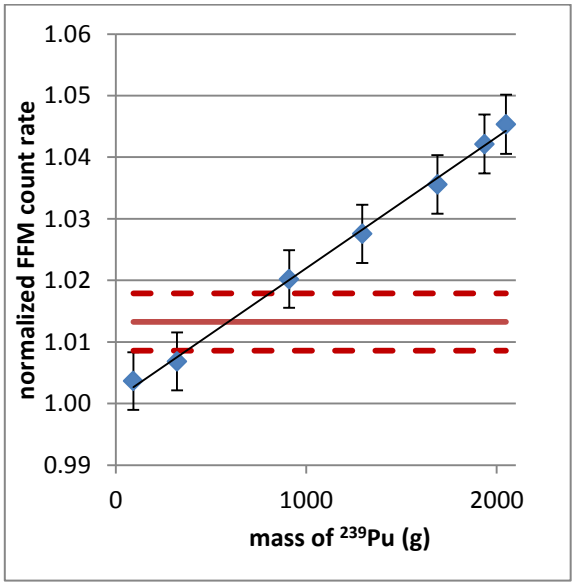

(c)

Figure 4.5. Normalized bare/FFM, Gd/bare and FFM count rate from the unknown Pu cylinder

Table 4.3 shows the ^{239}Pu content estimate for the unknown Pu cylinder using the results from the normalized bare/FFM and Gd/bare ratios separately, the weighted

average of the ratios estimates, the normalized FFM count rate alone, and finally the weighted average of the ratios and the count rate estimates. The result with the smallest percent difference compared to the theoretical mass of ^{239}Pu represented in bold is the best estimate of the fissile content of the unknown. These results show that the instrument is able to determine accurately the ^{239}Pu content of an artificial Pu cylinder. In addition, due to the linear trend of the normalized FFM count rate and the Gd/bare ratio as a function of ^{239}Pu content, the highest the fissile content, the lowest the relative uncertainty. Due to the logarithmic trend of the bare/FFM ratio, the results from this ratio only give more precise estimate for small ^{239}Pu content. Table 4.3 also shows that the comparison of the results from the two ratios can help increasing the accuracy of the estimate.

Table 4.3. Estimate of ^{239}Pu content for the unknown sample using different trends

Trend used	Unknown ^{239}Pu content estimate		
	mass (g)	uncertainty	% diff.
Bare/FFM	645.4	104.7	1.07 %
Gd/bare	574.3	346.0	10.07 %
Both ratios	**639.5**	**100.2**	**0.14 %**
FFM count rate	627.2	232.9	1.79 %
Ratios and count rate	637.6	92.0	0.19 %

4.2. Analysis of Cd-Ingot from Electrorefiner

The instrument response to irradiation of an artificial Pu cylinder has shown that it is capable to measure ^{239}Pu content of the cylinder with a relatively small uncertainty. To test the instrument on a realistic material from pyroprocessing process, simulations with Cd-ingot from the electrorefiner LLC have been performed. These simulations will

lead to conclusions about the capability of the instrument to measure ^{239}Pu content in pyroprocessing material.

4.2.1. EBR-II spent fuel isotopic composition

The characteristics of the Cd ingot from the Japan Atomic Energy Agency (JAEA) [40] were considered to perform MCNP simulation on a pyroprocessing material. The LCC used in JAEA was 2.5 cm in diameter. The Cd ingot obtained at the end of the electrorefining step contained 120 g of Cd and 14.7 g of Pu mixed with U [40]. The amount of each actinide in the metal product for Pu electrotransport is shown on Table 4.4. In order to get the isotopic composition of these actinides, a MCNPX burnup calculation was performed on an EBR-II model. It is assumed that the isotopic actinide composition in the Cd ingot is the same as the actinide composition of the EBR-II spent fuel.

Table 4.4. Actinide composition of the metal product for Pu electrotransport

Element	wt%
Uranium (U)	33.8
Neptunium (Np)	4.0
Plutonium (Pu)	55.6
Americium (Am)	6.4
Curium (Cm)	0.2

During its operation time, the EBR-II had been loaded with several type of fuel pin. To perform the burnup calculation, the Mark-V [48, 38] fuel type was used in an EBR-II MCNP model. Table 4.5 shows some characteristics of this type of fuel pin. The fuel rod is composed by U (63% enriched), Pu and zirconium (Zr) and is bonded by sodium for thermo-hydraulics purposes. An MCNP model of the EBR-II fuel pin is

shown on Figure C.1 in Appendix C. The model of the fuel pin has been designed with a 0.44-cm diameter fuel rod surrounded by 0.1 cm of sodium bond and with a 0.381-cm thick cladding. The core and its assemblies have a hexagonal lattice structure. The outside assemblies are made of depleted uranium and form the blanket. Pu is produced in the blanket during the reactor operation explaining the term breeder reactor: the reactor produces more Pu than it consumes. The EBR-II had been operated with different numbers of blanket and fuel assemblies, each containing 61 or 91 pins [49, 50]. For the purposes of the simulation, a small core representing an EBR-II MCNP model was created with 7 fuel assemblies and 12 blanket assemblies, each with 91 pins per assembly. This MCNP core model is shown on Figure C.2 in Appendix C. To obtain the regular 1% Pu in the blanket at discharge, as found in literature [48], a burnup calculation was performed on the MCNP model burning the fuel for 370 days at a power of 62.5 MW and letting it decay for 730 days. This simulation gave a typical actinide isotopic composition from irradiation of metal fuel in the EBR-II. This result is shown in Appendix D. Knowing that the Cd ingot is formed by 120 g of Cd and 14.7 g of Pu mixed with U with the same actinide isotopic composition of EBR-II spent fuel, the composition of the Cd ingot is deduced taking into account the data in Table 4.4.

Table 4.5. Characteristics of the Mark-V fuel pin

Fuel alloy (wt%)	U-20Pu-10Zr
Heavy metal density (g/cm^3)	14.1 – 14.3
Slug diameter (cm)	0.427 – 0.439
Plenum ot fuel volume ratio	1.45
Plenum gas	Argon
Cladding material	HT 9 steel
Pin length (cm)	34.3
Blanket	Depleted uranium (DU): UO_2 form

4.2.2. SINRD response to different ^{239}Pu content

To see how the material influenced the neutron flux originally transmitted by the source system, MCNP tally calculations have been performed after the Cd ingot; the Cd ingot bearing 50% of ^{239}Pu has been chosen as an example. The neutron fluxes before and after the material are shown on Figure 4.6. The two fluxes have a similar shape. However, the magnitude of the neutron flux after the material is lower due to absorption of neutrons in the Cd-ingot. The original flux is more depleted after the material for energies corresponding to the (Gd-Cd window) due to ^{239}Pu resonance at 0.3eV. It is also more depleted in the whole epithermal region due to the numerous resonances present in this energy group.

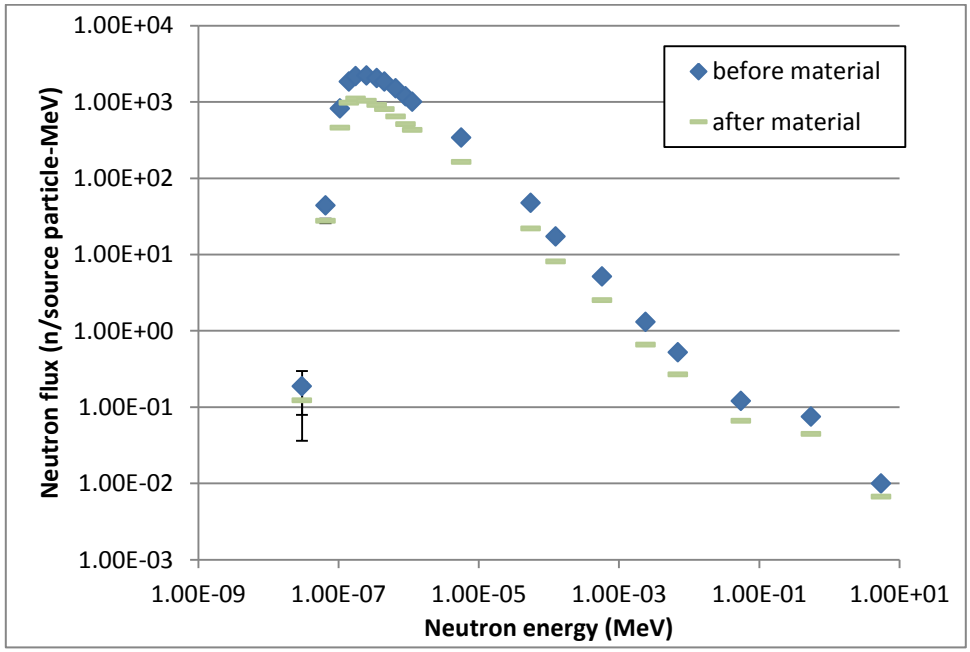

Figure 4.6. Neutron flux before and after the Cd ingot with 50 at% of ^{239}Pu

MCNP simulations have been run for several ^{239}Pu contents in the Cd ingot. The results from measurement of the Cd ingot without ^{239}Pu were used for normalization

purposes. Figure 4.7 show the configuration of the source, the detector, and the Cd ingot used for MCNP simulations. Over all ratios calculated from SINRD data, the normalized Cd/FFM and bare/FFM ratios provides the best SINRD signatures. Figure 4.8 shows these ratio plotted versus the ^{239}Pu content of the Cd ingot using: (1) U FCs for every detector of SINRD, and (2) U FCs for the bare and FFM detectors of SINRD and Pu FCs covered with Gd or Cd. Using U and Pu FCs instead of only U FCs increases SINRD signature by 50%: the slope of the Cd/FFM for U and Pu FCs is 1.5 times the slope for U FCs only. However, the bare/FFM ratio shows the same signature for U FCs or U and Pu FCs as U FCs are used in both cases for these two detectors. Thus, considering both Cd/FFM and bare/FFM ratios to measure the ^{239}Pu content of a Cd ingot, U and Pu FCs record the best SINRD signature.

On Figure 4.8, the Cd/FFM and bare/FFM ratios plateau out for a ^{239}Pu content superior to respectively 48 g and 67 g. This is due to shelf-shielding effects occurring from saturation of the large ^{239}Pu resonance at low energy. For a ^{239}Pu content greater than 48 g, the Cd/FFM ratio alone will not be sufficient to determine this fissile isotope content with a relatively small uncertainty (and similarly for 67 g with bare/FFM ratio); the normalized FFM count rate could then be used to confirm or determine the ^{239}Pu content of an ingot as its trend is linear as a function of the ^{239}Pu content; the graph of normalized FFM count rate versus ^{239}Pu content is shown on Figure 4.9. Comparing results from the two ratios and from the normalized FFM count rate makes possible to reduce the uncertainty of the estimate of ^{239}Pu content. According to the trend of the Cd/FFM and bare/FFM ratios versus the ^{239}Pu content, a measurement of an unknown Cd ingot with the instrument will give an estimate of the ^{239}Pu content with a relative uncertainty between 48 and 6 % (given that the uncertainty of the measurement is the same as the data points of the trend). When unable to use these two ratios, the normalized FFM will give an estimate of the ^{239}Pu content with a relative uncertainty between 21 and 8 %.

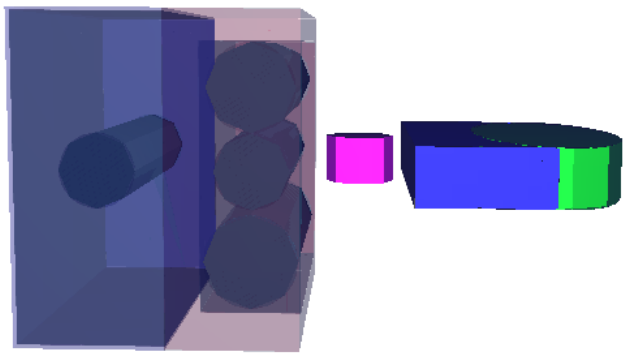

Figure 4.7. MCNP model of the measurement with Cd ingot

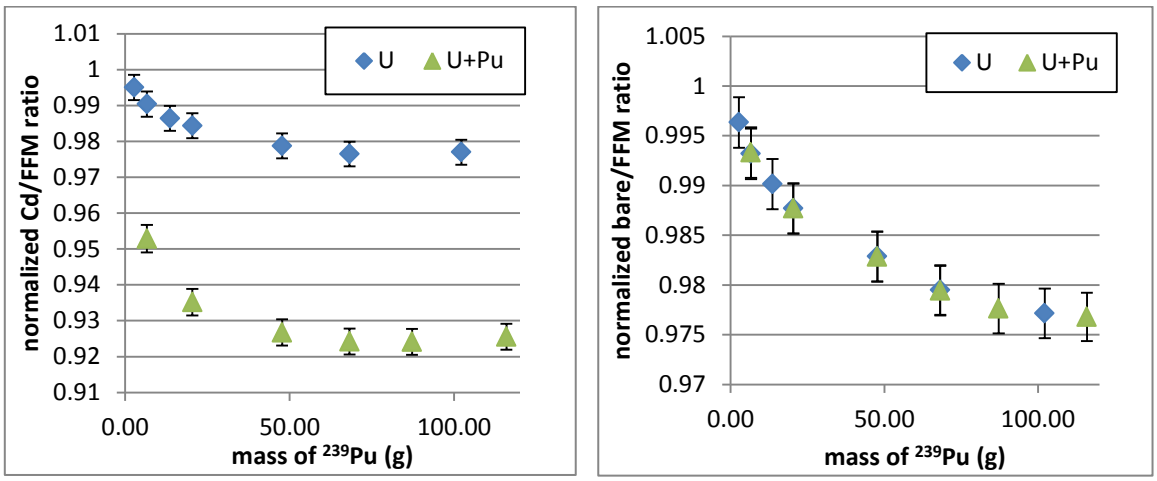

(a) (b)

Figure 4.8. Normalized (a) Cd/FFM ratio and (b) bare/FFM ratio from SINRD with U FCs only and U+Pu FCs for Cd ingot with different ^{239}Pu content

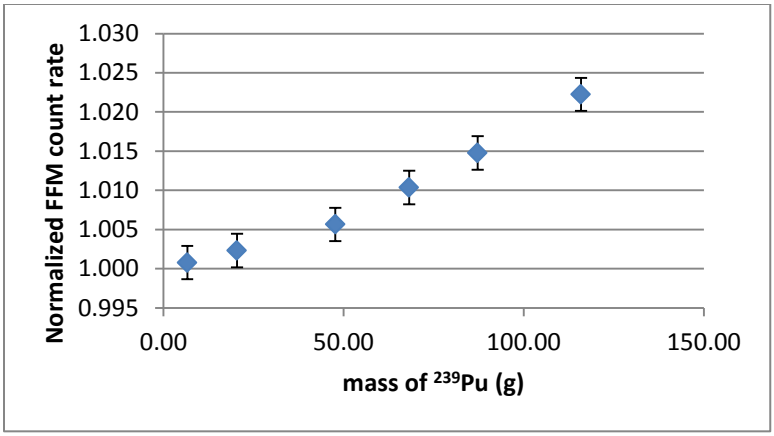

Figure 4.9. Normalized FFM count rate versus Cd ingot ^{239}Pu content

Test simulations have been run in MCNP to evaluate the precision of the ^{239}Pu content estimate from the normalized bare/FFM and Cd/FFM ratios, and normalized FFM count rate. Cd ingots containing respectively 13.6 and 102.2 g of ^{239}Pu have been simulated with the instrument and the SINRD ratios and count rates have been analyzed. The two samples are respectively called "unknown 1" and "unknown 2" in the following.

Figure 4.10 shows the data from the two unknowns plotted on the bare/FFM, Cd/FFM or normalized FFM count rate trends obtained from previous simulations; the top plots of the figure shows data from unknown 1 whereas the bottom ones are data from unknown 2. On the figure, the data from the unknowns has been represented by a plain red horizontal line; the dash lines represent the uncertainty associated with each data. To estimate the ^{239}Pu content of each sample, the smallest and highest masses corresponding to the data with their uncertainty have been calculated; the average of these two masses gives the estimate of the ^{239}Pu content and the difference between the masses and the average gives the uncertainty.

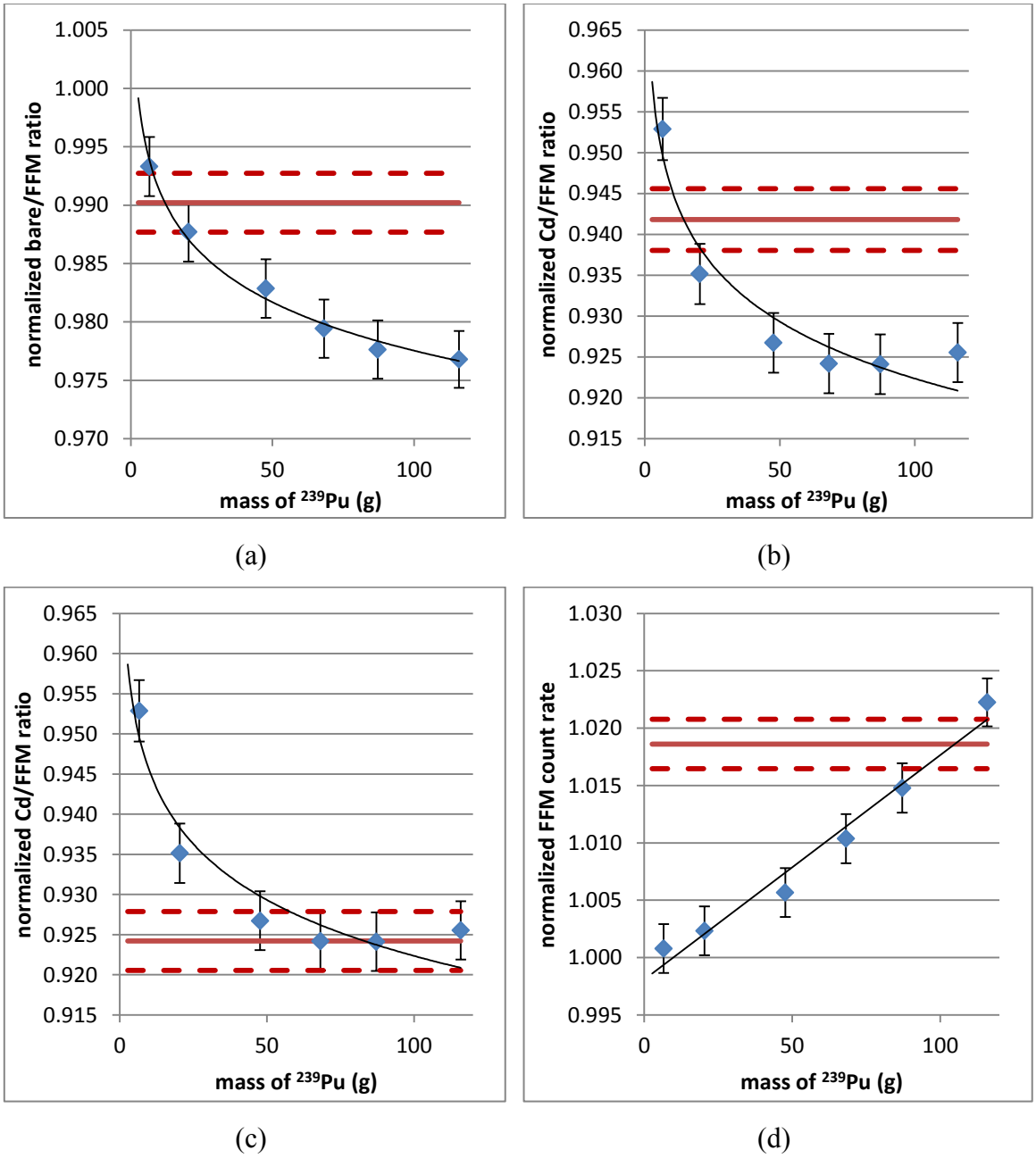

Figure 4.10. Analysis of data from unknown 1 ((a) and (b)) and unknown 2 ((c) and (d))

Table 4.6 shows the ^{239}Pu content estimate for the two unknowns using the results from the bare/FFM and Cd/FFM ratios separately, their weighted average, the

normalized FFM count rate alone, and finally the weighted average of the ratios and the count rate estimates. The result with the smallest percent difference compared to the theoretical mass of ^{239}Pu represented in bold is the best estimate of the fissile content of the unknowns. These results show that the instrument is able to determine accurately the ^{239}Pu content of a Cd ingot; in addition, due to the linear trend of the normalized FFM count rate as a function of ^{239}Pu content, the highest the fissile content, the lowest the relative uncertainty. Due to the logarithmic trend of the ratios, the results from the ratios only are more precise than from the normalized FFM count rate for small ^{239}Pu content. Table 4.6 also shows that the comparison of the results from the two ratios helps increasing the accuracy of the estimate.

Table 4.6. Estimate of unknowns' ^{239}Pu content for several trends

Trend used	Unknown 1 ^{239}Pu content estimate			Unknown 2 ^{239}Pu content estimate		
	mass (g)	uncertainty	% diff	mass (g)	uncertainty	% diff
Bare/FFM	13.0	5.2	4.25%	116.9	45.9	14.40%
Cd/FFM	15.6	5.6	15.04%	90.4	31.6	13.06%
Both ratios	**14.2**	**3.8**	**4.58%**	98.9	26.0	3.21%
FFM count rate	15.9	10.6	17%	102.6	10.8	0.38%
Ratios and count rate	14.4	3.6	6%	**102.1**	**10.0**	**0.14%**

In summary, the simulations of the instrument measuring Cd ingots with different ^{239}Pu content have shown that the normalized bare/FFM and the Cd/FFM ratios show the best SINRD signature. Due to their logarithmic trend, these ratios estimate large fissile contents with large uncertainties. To decrease these uncertainties in estimate, the normalized FFM count rate can be used. In addition, decreasing the uncertainty of the measurement by increasing the counting time and/or the source strength will contribute to decrease the uncertainty of the ^{239}Pu content estimate.

5. CONCLUSIONS

The results from MCNP simulations and experimental measurements were used to investigate the use of SINRD to quantify ^{239}Pu in the pyroprocessing process for safeguards purposes. The purpose of these simulations and measurements was to: (1) design an instrument using SINRD and (2) evaluate the capability of the instrument to measure fissile content in pyroprocessing material. The instrument is composed by a neutron source pod, creating a 1/E slowing down function to interrogate a material, and SINRD detector pod. SINRD uses ratios of different detectors to cancel most of the systematic errors related to calibration and positioning.

From comparison between MCNP simulations and measurements using fresh fuel in a form of U cans, it has been concluded that the MCNP models accurately simulate the physics of the experiment. As fresh fuel contains a fissile isotope with a resonance at 0.3 eV (^{235}U), the instrument behavior with fresh fuel is expected to be the same as measuring spent fuel. A good agreement between results from simulations and measurements was only possible when the data was normalized to the empty can case: the normalization of SINRD results with a reference object of similar geometry is necessary to cancel bias errors and get accurate data. The normalized bare/FFM and Gd/bare ratios have been determined as the best SINRD signatures for quantification of ^{235}U in U cans. These results have been obtained using ^{3}He tubes in the detector pod. Even if this type of detectors does not contain a fissile isotope sensitive to the fissile content of the interrogated material, its high efficiency makes possible to obtain usable data.

Simulations on an artificial Pu cylinder and on a Cd ingot comparable to a pyroprocessing electrorefiner product were performed for various ^{239}Pu contents. The SINRD ratios which showed the best signature for quantification of ^{239}Pu content in Cd ingot were the normalized bare/FFM and the Cd/FFM ratios. Both ratios level off for the highest ^{239}Pu simulated due to saturation of the low-energy resonance of the fissile isotope. However, when an unknown is measured and analyzed using these ratios, the

weighted average of the different estimates makes it possible to reduce the uncertainty of the estimate. In addition, normalized count rate trend could also be used to determine, confirm or improve the estimate of fissile content in a material.

The two simulations with unknown Cd ingots have shown that the SINRD instrument is capable of determining ^{239}Pu content of the material, with relatively small uncertainties. However, improvements on the fissile content estimation will be possible by: (1) improving the trend of the normalized ratios by using more data points; (2) reducing the data point's uncertainties by simulating more particles; and (3) reducing the measurement uncertainty of an unknown by simulating more particles. Experimentally, these improvements would be possible by increasing the source strength of the Cf sources used and/or increasing the counting time.

An alternative design of the SINRD detector pod would be to use parallel FC plates. This design, similar to the one used in the 1969 SINRAD experiment [35], would considerably reduce the errors due to geometric setup of the instrument: each FCs would have same entering neutron flux. The bare FC plate would be the first one to detect neutrons; then, the Gd FC would detect neutrons of energy higher than 0.13 eV; the following Cd FC would detect neutrons of energy higher than 0.25 eV; finally a B_4C FC will detect the fast neutrons of energy higher than 3.8 keV. This design would possibly make the normalization to object of similar dimensions not mandatory.

This research has led to the conclusion that the SINRD instrument is a candidate for safeguarding pyroprocessing facilities. Future work includes performing experimental measurements using FCs, simulating the instrument response to other pyroprocessing materials, building a remote control prototype of the instrument for measurements in hot cells, and performing additional verification measurements on pyroprocessing material. Finally, the prototype of the instrument would have to be optimized to be used for safeguards.

REFERENCES

[1] M. F. Simpson, "Developments of Spent Nuclear Fuel Pyroprocessing Technology at Idaho National Laboratory," Idaho National Laboratory, INL/EXT-12-25124, Idaho Falls, ID, USA, March 2012.

[2] M. F. Simpson, "Sustainable Nuclear Power via Implementation of a Closed Fuel Cycle," Idaho National Laboratory, Presentation for Nuclear Science and Engineering Directorate, Educational Outreach, Oak Ridge, TN, USA, June 22, 2011.

[3] IAEA, "Spent Fuel Reprocessing Options," International Atomic Energy Agency, IAEA-TECDOC1587, Vienna, Austria, August 2008.

[4] B. P. Reddy, K. Nagarajan, P. R. V. Rao, B. Raj, "Current Status of Pyroprocess Development at IGCAR, Kalpakkam, India," in *The 3rd International Pyroprocessing Research Conference*, Dimitrovgrad, Russia, November 29 - December 3, 2010.

[5] R. Bean, "Project Report on Development of a Safeguards Approach for Pyroprocessing," Idaho National Laboratory, INL/EXT-10-20057, Idaho Falls, ID, USA, September 2010.

[6] H. Yamana, "Pyrochemical Reprocessing Developments in Japan - Overview and Some Topics," in *Nuclear Fuel Cycle Technologies: Closing the Fuel Cycle*, B. Raj and P. R. V. Rao, Eds., Kalpakkam, Tamilnadu, India, Board of Research in Nuclear Sciences, Department of Atomic Energy, 2007.

[7] J. Lacquement, S. Bourg, H. Boussier, O. Conocar, A. Laplace, P. Baron, A. Grandjean, D. Warin, B. Boullis, "Pyrochemistry Assessment at CEA - Last Experimental Results," in *Global 2007: Advanced Nuclear Fuel Cycles and Systems*, Boise, ID, USA, September 9-13, 2007.

[8] S. Bourg, C. Hill, C. Caravaca, C. Rhodes, C. Ekberg, et al., "Pyroprocessing Achievements in the filed of the ACSEPT Projet," in *The 3rd International*

Pyroprocessing Research Conference, Dimitrovgrad, Russia, November 29 - December 3, 2010.

[9] OECD - NEA, "Pyrochemical Separations in Nuclear Applications," OECD Publications, ISBN 92-64-02071-3, Paris, France, 2004.

[10] J. J. Laidler, J. E. Battles, W. E. Miller, J. P. Ackerman, E. L. Carls, "Development of Pyroprocessing Technology," *Progress in Nuclear Energy,* vol. 31, no. 1/2, pp. 131-140, 1997.

[11] J.-H. Yoo, C.-S. Seo, E.-H. Kim, H.-S. Lee, "A Conceptual Study of Pyroprocessing for Recovering Actinides from Spent Oxide Fuels," *Nuclear Engineering and Technology,* vol. 40, no. 7, pp. 581-592, December 2008.

[12] T. Inoue, T. Koyama, Y. Arai, "State of the Art of Pyroprocessing Technology in Japan," *Energy Procedia,* vol. 7, pp. 405-413, 2011.

[13] H. Lee, "Pyroprocessing Technology Development at KAERI," in *The 3rd International Pyroprocessing Research conference*, Dimitrovgrad, Russia, November 29 - December 3, 2010.

[14] R. W. Benedict, C. Solbrig, B. Westphal, T. A. Johnson, S. X. Li, K. Marsden, K. M. Goff, "Pyroprocessing Progress at Idaho National Laboratory," Idaho National Laboratory, INL/CON-07-12983, Idaho Falls, ID, USA, September 2007.

[15] M. F. Simpson, T.-S. Yoo, R. W. Benedict, S. Phongikaroon, S. Frank, P. Sachdev, K. Hartman, "Strategic Minimization of High Level Waste from Pyroprocessing of Spent Nuclear Fuel," Idaho National Laboratory, INL/CON-07-12123, Idaho Falls, ID, USA, September 2007.

[16] IAEA, "The Structure and Content of Agreements Between the Agency and States Required in Connection with the Treaty on the Non-Proliferation of Nuclear Weapons, INFCIRC/153 (Corrected)," International Atomic Energy Agency, Vienna, Austria, June 1972.

[17] IAEA, "Safeguards Glossary," International Atomic Energy Agency, Vienna, Austria, 2001 Edition.

[18] A. M. LaFleur, "Development of Self-Interrogation Neutron Resonance Densitometry (SINRD) to Measure the Fissile Content in Nuclear Fuel," Texas A&M University, Ph. D Dissertation, College Station, TX, USA, August 2001.

[19] M. F. Simpson, J. D. Law, "Nuclear Fuel Reprocessing," Idaho National Laboratory, INL/EXT-10-17753, Idaho Falls, ID, USA, 2010.

[20] T. Inoue, "An Overview of CRIEPI Pyroprocessing Activities," in *9th OECD/NEA P&T IEM*, Nimes, France, September 25-29, 2006.

[21] E. J. Karell, K. V. Gourishankar, J. L. Smith, L. S. Chow, L. Redey, "Separation of Actinides from LWR Spent Fuel using Molten-Salt-Based Electrochemical Processes," *Nuclear Technology,* vol. 136, pp. 342-353, December 2001.

[22] H.-D. Kim, "Development of Safeguards Approach for Reference Engineering-scale Pyroprocessing facility," in *International Pyroprocessing Research Conference*, Fontana-On-Geneva Lake, WI, USA, August 26-29, 2012.

[23] P. C. Durst, I. Therios, R. Bean, A. Dougan, B. D. Boyer, R. Wallace, M. Ehinger, D. Kovacic, K. Tolk, "Advanced Safeguards Approaches for New Reprocessing Facilities," Pacific Northwest National Laboratory, PNNL-16674, Richland, WA, USA, June 2007.

[24] P. C. Durst, R. Bean, M. H. Ehinger, A. Dougan, B. Boyer, K. Tolk, I. Therios, "Advanced Safeguards Approaches for New TRU Fuel Fabrication Facilities," Pacific Northwest National Laboratory, Richland, WA, USA, 2007.

[25] H. Kim, H. S. Shin, S. K. Ahn, "Status and Prospect of Safeguards by Design for the Pyroprocessing Facility," in *International Atomic Energy Agency Safeguards Symponium*, Vienna, Austria, October 31 - November 5, 2010.

[26] X-5 Monte Carlo Team, "MCNP - A General Monte Carlo N-Particle Transport Code, Version 5," Volume 1 & 2, Los Alamos National Laboratory, Los Alamos, NM, USA, April 24, 2003.

[27] N. N. Das Gupta, S. K. Ghosh, "A Report on the Wilson Cloud Chamber and Its Applications in Physics," *Reviews of Modern Physics,* vol. 18, no. 2, pp. 225-284,

April 1946.

[28] D. Gerts, M. Paff, R. Bean, "Nuclear Material Accountability Applications of a Continuous Energy and Direction Gamma Ray Detector," in *INMM Annual Meeting*, Baltimore, MD, USA, July 11-15, 2010.

[29] D. Gerts, H. Wimberly, N. Fredette, "Using GPU Programming for Inverse Spectroscopy," in *INMM Annual Meeting*, Baltimore, MD, USA, July 11-15, 2010.

[30] K. Zhao, M. Penkin, C. Norman, S. Balsley, K. Mayer, et al., "International Target Values 2010 for Measurement Uncertainties in Safeguarding Nuclear Materials," International Atomic Energy Agency, STR-368, Vienna, Austria, November 2010.

[31] H. L. Chang, F. X. Gao, W. I. Ko, H. D. Kim, S. Y. Lee, "Evaluation of Sigma-MUF (Material Unaccounted For) for the Conceptually Designed Korea Advanced Pyroprocess Facility," *Journal of the Korean Physical Society,* vol. 59, no. 2, pp. 1418-1421, August 2011.

[32] S. Y. Lee, K. E. Thomas, J. B. Marlow, H. O. Menlove, W .I. Ko, M. S. Yang, S. W. Park, "A Preliminary Study on the Safeguardability of a Korean Advanced Pyroprocessing Facility (KAPF)," in *Global 2007: Advanced Nuclear Fuel Cycles and Systems*, Boise, ID, USA, September 9-13, 2007.

[33] B. B. Cipiti, F. A. Duran, B. Key, Y. Liu, I. Lozano, R. Ward, "Modeling and Design of Integrated Safeguards and Security for an Electrochemical Reprocessing Facility," Sandia National Laboratories, SAND2012-9303, Albuquerque, NM, USA, 2012.

[34] A. M. LaFleur, W. S. Charlton, H. O. Menlove, M. Swinhoe, "Nondestructive Measurements of Fissile Material using Self-Indication Neutron Resonance Absorption Densitometry (SINRAD)," in *Proceedings of the 8th International Conference on Facility Operations - Safeguards Interface*, Portland, OR, USA, March 30 - April 4, 2008.

[35] H. O. Menlove, C. D. Tesche, M. M. Thorpe, R. B. Walton, "A Resonance Self-Indication Technique for Isotopic Assay of Fissile Materials," *Nucl. Appl.,* vol. 6,

pp. 401-408, April 1969.

[36] T. W. Crane, M. P. Baker, "Neutron Detectors," in *Passive Nondestructive Assay of Nuclear Materials*, Washington, DC, USA, United States Nuclear Regulatory Commission, 1991, pp. 379-406.

[37] OECD Nuclear Energy Agency, "Janis 3.4 User's Guide," OECD NEA, Issy-les-Moulineaux, France, May 2012.

[38] W. J. Carmack, D. L. Porter, Y. I. Chang, S. L. Hayes, M. K. Meyer, et al., "Metallic Fuels for Advanced Reactors," *Journal of Nuclear Materials,* vol. 392, pp. 139-150, 2009.

[39] Los Alamos National Laboratory, "MCNPx User's Manual, Version 2.7.0," Los Alamos National Laboratory, LA-CP-11-00438, Denise B. Relowitz, Ed., Los Alamos, NM, USA, April 2011.

[40] T. Inoue, T. Koyama, M. Myochin, Y. Arai, "Pyroprocessing Technology Development in Japan," in *Global 2007: Advanced Nuclear Fuel Cycles and Systems*, Boise, ID, USA, September 9-13, 2007.

[41] LND, INC., Designers and Manufacturers of Nuclear Radiation Detectors, [Online]. Available: http://www.lndinc.com/.

[42] B. S. Carpenter, J. W. Gramlich, R. R. Greenberg, L. A. Machlan, P. DeBievre, et al., "Uranium-235 Isotope Abundance Standard Reference Materials for Gamma Spectrometry Measurements," U.S. Department of Commerce/National Bureau of Standards, NBS Special Publication 260-96, Gaithersburg, MD, USA, 1986.

[43] P. Matussek, "Accurate Determination of the 235U Isotope Abundance by Gamma Spectrometry - A User's Manual for the Certified Reference Material EC-NRM-171/NBS-SRM-969," Kernforschungszentrum Karlsruhe GmbH, Karlsruhe, Germany, May 1985.

[44] Canberra Industries, Inc., "Lynx Digital Signal Analyzer - User's Manual," Canberra Industries, Inc., Meriden, CT, USA, 2011.

[45] Canberra Industries, Inc., "Genie 2000 Spectroscopy Software - Operations," Canberra Industries, Inc., Meriden, CT, USA, 2006.

[46] G. F. Knoll, "Chapter 14: Slow Neutron Detection Methods," in *Radiation Detection and Measurement*, Third ed., Ann Harbor, MI, USA, John Wiley & Sons, Inc., 2000.

[47] A. Croff, "A User's Manual for the ORIGEN2 Computer Code," Oak Ridge National Laboratory, Oak Ridge, TN, USA, 1980.

[48] M. J. Lineberry, H. F. McFarlane, "The EBR-II Spent Fuel Treatment Program," in *GLOBAL '95 International Conference*, Versailles, France, 1995.

[49] J. Case, "Core-Loading Diagrams for EBR-II Runs 4 through 38," Argonne National Laboratory, Idaho Falls, ID, USA, 1969.

[50] D. E. Burkes, R. S. Fielding, D. L. Porter, D. C. Crawford, M. K. Meyer, "A US Perspective on Fast Reactor Fuel Fabrication Technology and Experience Part I: Metal Fuels and Assembly Design," *Journal of Nuclear Materials,* vol. 389, pp. 458-469, 2009.

[51] A. Borella, R. Rossa, K. Van Der Meer, "Modelling of high enriched uranium fission chamber with the code MCNPX," in *35th annual ESARDA Symposium on International Safeguards*, Bruges, Belgium, May 27-30, 2013.

APPENDIX A. DRAWINGS FOR THE DETECTOR POD PROTOTYPE MACHINING

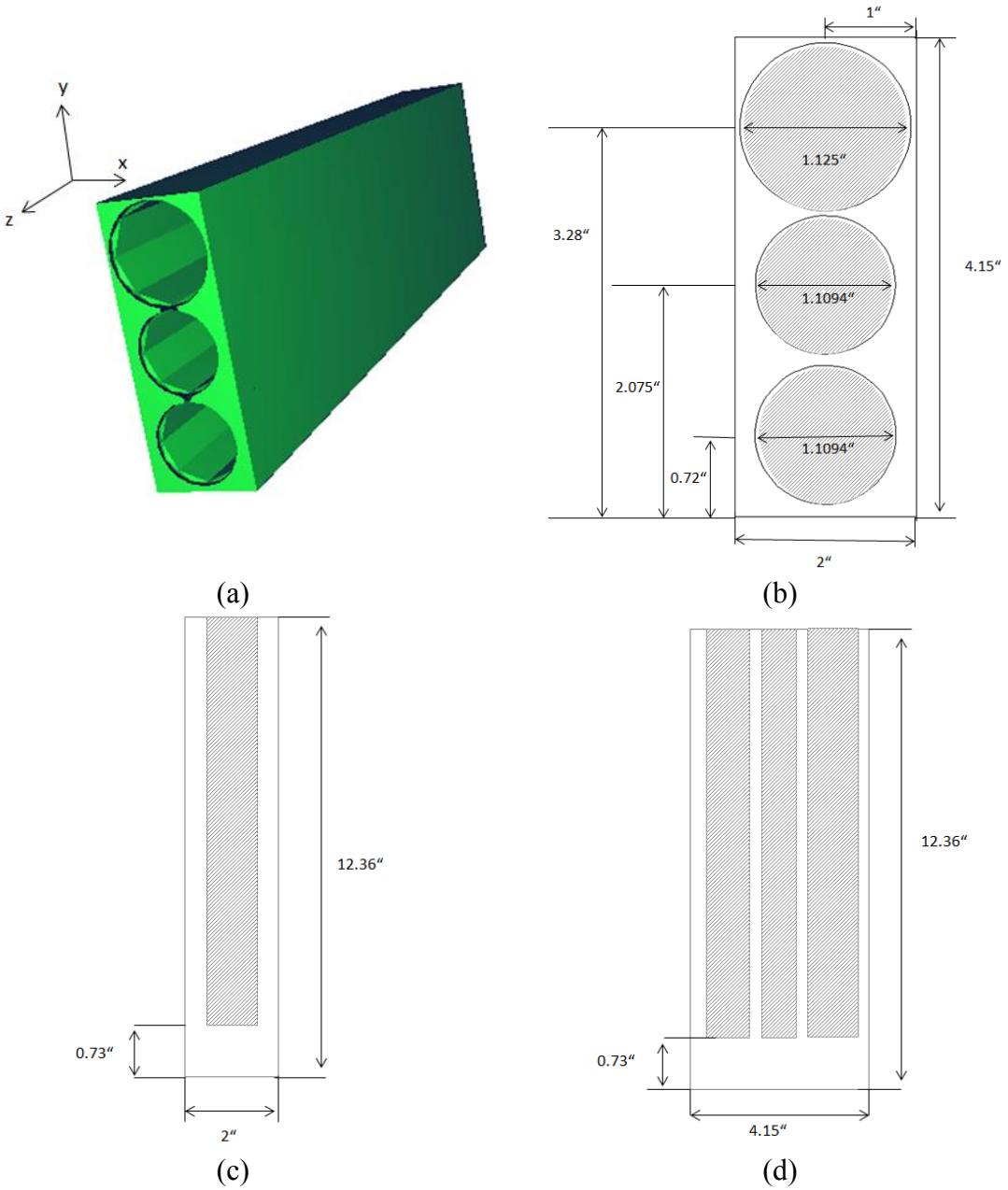

Figure B.1. Drawings for Al block machining: (a) 3-D view, (b) x-y view, (c) x-z view and (d) y-z view

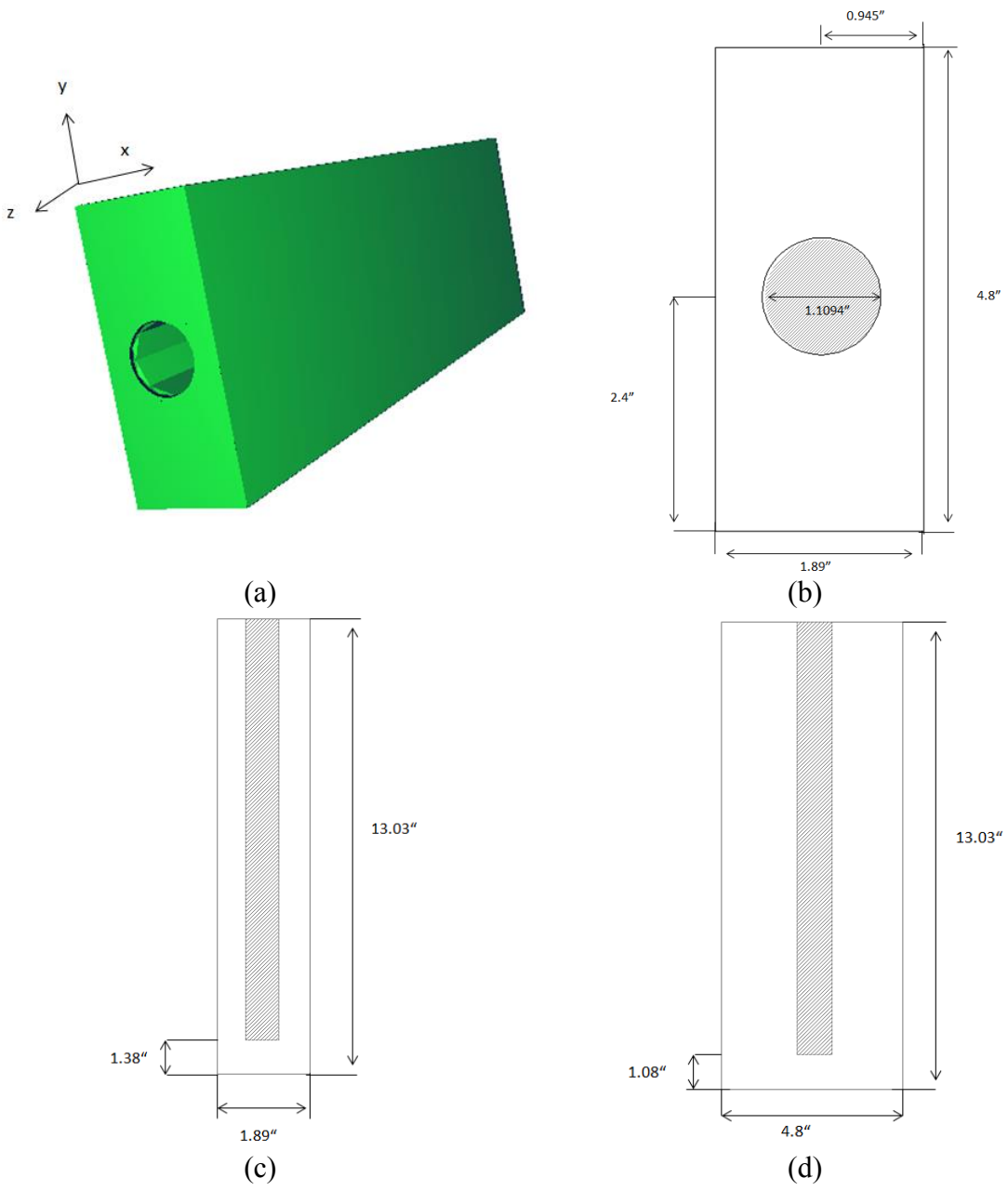

Figure B.2. Drawings for UHMWPE block machining: (a) 3-D view, (b) x-y view, (c) x-z view and (d) y-z view

APPENDIX B. EXAMPLE OF MCNP INPUT FILE

```
test instrument with U-can 2.95% U235 and lab FC
c
c ============ CELL CARDS ======================
c
c
c ---------- neutron source -----------
100   4   -0.940  -100 +110 -111                        imp:n=1   $ Poly
101   3   -8.908  -103 +104 +100 +110 -111 -105 +101   imp:n=1   $ Ni
102   0           -103 +104 -101 +102 +110 -111 imp:n=1  $ Gd if needed
c
c ---------- U can 200.1g U3O8-----------
200   22 -2.6   -201                 imp:n=1
201   0         -202                 imp:n=1
202   0         -203                 imp:n=1
203   18 -6.826 -200 +201 +202 +203  imp:n=1
c
c ----------- detector --------------
300   14  -2.70  -300 +312 +333 +343 #304 #306 #307 #313 #323 #334 #344
&  imp:n=1 trcl=1 $ Al box
301    13  -1.45  -301 +300 #343 #304 #306 #307 imp:n=1 trcl=1 $ 1.0cm
B4C Liner
302   4   -0.94   -303 +322  +323 #305    imp:n=1 trcl=1  $ Poly Box
303   2   -8.65   -302 +303  #305         imp:n=1 trcl=1 $ 1mm Cd Liner
304   0           -304 +312 +313                imp:n=1 trcl=1
305   0           -305 +322 +323                imp:n=1 trcl=1
306   0           -306 +333 +334                imp:n=1 trcl=1
307   0           -307 +343 +344                imp:n=1 trcl=1
c bare U235 fission chamber
310   24  -0.0059268  -310                 imp:n=1 trcl=1
311   15  -19.1       -311 +310           imp:n=1 trcl=1
312   14  -2.70       -312 +311           imp:n=1 trcl=1
313   14  -2.70       -313                imp:n=1 trcl=1
c FFM U235 fission chamber
320   24  -0.0059268  -320                 imp:n=1 trcl=1
321   15  -19.1       -321 +320           imp:n=1 trcl=1
322   14  -2.70       -322 +321           imp:n=1 trcl=1
323   4   -0.94       -323                imp:n=1 trcl=1
c 0.1mm Gd covered U235 fission chamber
330   24  -0.0059268  -330                 imp:n=1 trcl=1
331   15  -19.1       -331 +330           imp:n=1 trcl=1
332   14  -2.70       -332 +331           imp:n=1 trcl=1
333   5   -7.90       -333 +332           imp:n=1 trcl=1
334   14  -2.70       -334                imp:n=1 trcl=1
c 3.0mm Cd covered U235 fission chamber
340    24  -0.0059268 -340                imp:n=1 trcl=1
341    15 -19.1       -341 +340           imp:n=1 trcl=1
342    14 -2.70       -342 +341           imp:n=1 trcl=1
343    2  -8.65       -343 +342           imp:n=1 trcl=1
344    14 -2.70       -344                imp:n=1 trcl=1
c
```

```
c ----------- tallies ---------------
c 400    0     +13 -102 -103 +104 +110 -111       imp:n=1 $ SSW surface
c
c ---------- vacuum -----------------
900    0    -900 +200 #100 #101 #102 #300 #301 #302 #303 #304 #305 #306
& #307 #310 #311 #312 #313 #320 #321 #322 #323 #330 #331 #332
& #333 #334 #340 #341 #342 #343 #344 imp:n=1
901    0     +900                              imp:n=0

c
c =========== SURFACE CARDS ====================
c
c
c ---------- neutron source surfaces ----------
100     SQ   +0.15 +0.03 0 0 0 0 -1 0 0 0
101     PX   -5
102     PX   -5.01                          $ surface of the source
103     PY   +5.7
104     PY   -5.7
105     PX   +0.0
110     PZ   -6
111     PZ   6
c
c --------- U can surfaces -----
200     RCC   -9.51 0 -1.239 0 0 8.898 3.5
201     RCC   -9.51 0 -1.039 0 0 2.078 3.4935
202     RCC   -9.51 0  4.039 0 0 2.42  3.3
203     RCC   -9.51 0  6.459 0 0 1.2   3.4935
c
c ------------ detector surfaces --------------
c Detector box
300    RPP  -17.45 -13.91 -16.08 16.08  -4.925 4.60
301    RPP  -18.45 -13.91 -17.08 17.08  -5.925 5.60
302    RPP  -23.35 -18.45 -17.08 17.08  -5.925 5.60
303    RPP  -23.25 -18.45 -16.98 16.98  -5.825 5.50
c holes to insert detectors
304    RCC  -15.68 -14.225  0    0 31.305 0 1.37
305    RCC  -20.80 -14.225  0    0 31.305 0 1.37
306    RCC  -15.68 -14.225  2.98 0 31.305 0 1.38
307    RCC  -15.68 -14.225 -3.14 0 31.305 0 1.67
c Bare U235 fission chamber
310    RCC  -15.68 -6.35 0 0 12.70 0 1.179996
311    RCC  -15.68 -6.35 0 0 12.70 0 1.18
312    RCC  -15.68 -7.81 0 0 15.62 0 1.27
313    RCC  -15.68 -14.225 0 0 6.415 0 1.27
c FFM fission chamber
320    RCC  -20.80 -6.35 0 0 12.70 0 1.179996
321    RCC  -20.80 -6.35 0 0 12.70 0 1.18
322    RCC  -20.80 -7.81 0 0 15.62 0 1.27
323    RCC  -20.80 -14.225 0 0 6.415 0 1.27
c 0.1mm Gd covered fission chamber
330    RCC  -15.68 -6.35  2.98 0 12.7  0 1.179955
331    RCC  -15.68 -6.35  2.98 0 12.7  0 1.18
332    RCC  -15.68 -7.81  2.98 0 15.62 0 1.27
```

```
333    RCC  -15.68 -7.81  2.98 0 15.62 0 1.28
334    RCC  -15.68 -14.225 2.98 0 6.415 0 1.28
c 3.0mm Cd covered fission chamber
340    RCC -15.68 -6.35 -3.14 0 12.7  0 1.179955
341    RCC -15.68 -6.35 -3.14 0 12.7  0 1.18
342    RCC -15.68 -7.81 -3.14 0 15.62 0 1.27
343    RCC -15.68 -7.81 -3.14 0 15.62 0 1.57
344    RCC -15.68 -14.225 -3.14 0 6.415 0 1.57
c
c --------- surfaces for tallies --------------
13     PX   -5.51                          $ plane for SSW/SSR
c
c --------- surface for outside world -----------------
900     so   +100

c
c ========== DATA CARDS ========================
c
c
c -------- Source definition -----------
MODE N
SDEF ERG=D1 POS=D2 $ 2 point Cf sources, position 4.58 or -4.58
SP1   -3 1.025 2.926      $ distribution for Cf n source
SI2   L 0 4.58 0 0 -4.58 0
SP2   D 1 1
c SSR   PTY=N
c
c -------- Materials -----------------
c **** natural cadmium 8.65g/cc ****
m2    48106.66c 0.012500
      48108.66c 0.008900
      48110.66c 0.124900
      48111.66c 0.128000
      48112.66c 0.241300
      48113.66c 0.122200
      48114.66c 0.287300
      48116.66c 0.074900
c **** natural nickel 8.908g/cc ****
m3    28058.66c 0.680770
      28060.66c 0.262230
      28061.66c 0.011400
      28062.66c 0.036340
      28064.66c 0.009260
c **** polyethylene C2H4 0.94g/cc ****
m4     1001.66c 0.666567
       1002.66c 0.000100
       6000.66c 0.333333
mt4    poly.10t
c **** natural gadolinium 7.90g/cc ****
m5    64152.66c 0.0020
      64154.66c 0.0218
      64155.66c 0.1480
      64156.66c 0.2047
      64157.66c 0.1565
```

```
      64158.66c 0.2484
      64160.66c 0.2186
c **** plutonium after irradiation ****
m6    94238.66c 0.00079
      94239.66c 0.75611
      94240.66c 0.15055
      94241.66c 0.08363
      94242.66c 0.00893
m7    94239.66c 1.0      $ Pu239
m8    94238.66c 1.0
m9    94240.66c 1.0
m10   94241.66c 1.0
m11   94242.66c 1.0
c **** natural hafnium 13.31g/cc ****
m12   72174.66c 0.00162
      72176.66c 0.05206
      72177.66c 0.18606
      72178.66c 0.27297
      72179.66c 0.13629
      72180.66c 0.35100
c ------- natural boron carbide powder d=1.02g/cc------
m13  5010.66c 0.796
     5011.66c 3.204
     6000.66c 1.0
c **** aluminum 2.7g/cc ****
m14   13027.66c 1.0
mt14  al27.12t
c **** 93% U235 ****
m15   92235.66c 0.93
      92238.66c 0.07
c **** steel 8g/cc ****
m16   24000.50c 1.7385e-2
      26000.50c 5.9206e-2
      28000.50c 7.6995e-3
      25055.66c 1.7320e-3
c **** Cd-U-Pu ingot 16.63g/cc******
m17   92233 -0.00001
      92234 -0.02625
      92235 -2.32253
      92236 -0.17970
      92238 -1.54901
      93236.70c -0.00006
      93237 -0.38558
      94238 -0.01194
      94239 -4.86726
      94240 -1.38619
      94241 -0.34246
      94242 -0.09883
      95241 -0.71767
      95242 -0.00216
      95243 -0.05219
      96242 -0.00381
      96243 -0.00053
      96244 -0.01918
```

```
      96245 -0.00060
      96246 -0.00001
      48106 -1.03675
      48108 -0.75209
      48110 -10.75008
      48111 -11.11726
      48112 -21.14647
      48113 -10.80493
      48114 -25.62783
      48116 -6.79865
      nlib=66c
c
c ------- aluminum can d=6.836g/cc -----
m18   13027.70c -97.35975
      14000.60c -0.4
      29000.50c -0.15
      24000.50c -0.04
      12000.66c -0.8
      26000.55c -0.7
      30000.70c -0.25
      25055.70c -0.15
      22000.66c -0.15
      23000.70c -0.00025
mt18  al27.12t
c ----- 0.31% U235 U3O8 d=2.6g/cc ----
m19   92235.70c -0.00260
      92238.70c -0.84545
       8016.70c -0.15196
c ----- 0.71% U235 U3O8 d=2.6g/cc ----
m20   92235.70c -0.00595
      92238.70c -0.84209
       8016.70c -0.15196
c ----- 1.94% U235 U3O8 d=2.6g/cc ----
m21   92235.70c -0.01625
      92238.70c -0.83177
       8016.70c -0.15198
c ----- 2.95% U235 U3O8 d=2.6g/cc ----
m22   92235.70c -0.02471
      92238.70c -0.82329
       8016.70c -0.15200
c ----- 4.46% U235 U3O8 d=3.47g/cc ----
m23   92235.70c -0.03736
      92238.70c -0.81061
       8016.70c -0.15202
c ------- P10 gas d=0.0059268g/cc -----
m24    18000.59c 0.9
       6000.70c 0.02
       1001.70c 0.08
c ---rotation -----
*tr1= 0 0 0 0 90 90 90 90 0 90 180 90
c ------ Flux tallies for calculation of fission rate in FC ---------
F4:n   311
FM4   (-1 15 -6)
SD4    1
```

```
F14:n  321
FM14  (-1 15 -6)
SD14   1
F24:n  331
FM24   (-1 15 -6)
SD24    1
F44:n  341
FM44  (-1 15 -6)
nps    1e9
```

APPENDIX C. MCNP MODEL OF THE EBR-II FOR BURNUP CALCULATION

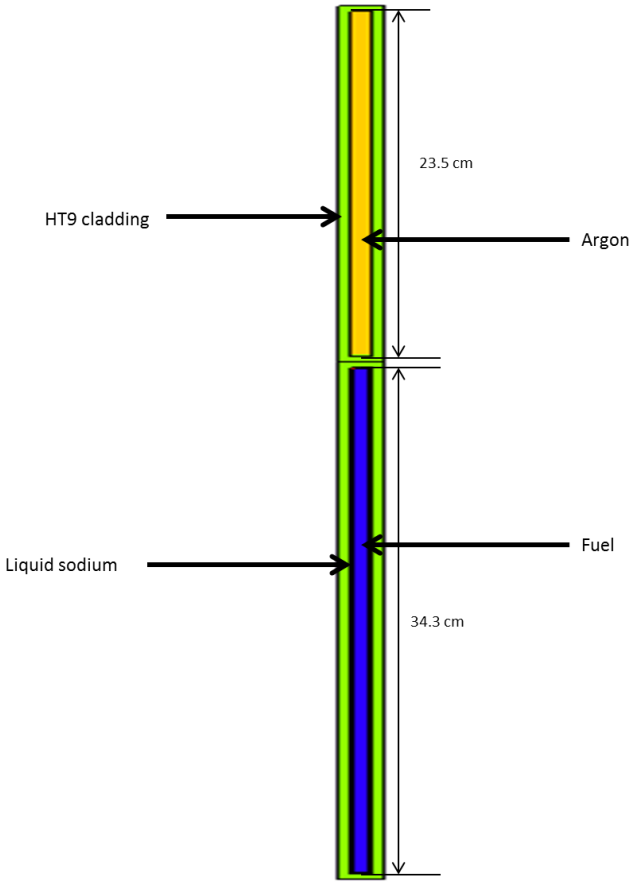

Figure C.1. EBR-II fuel pin MCNP model

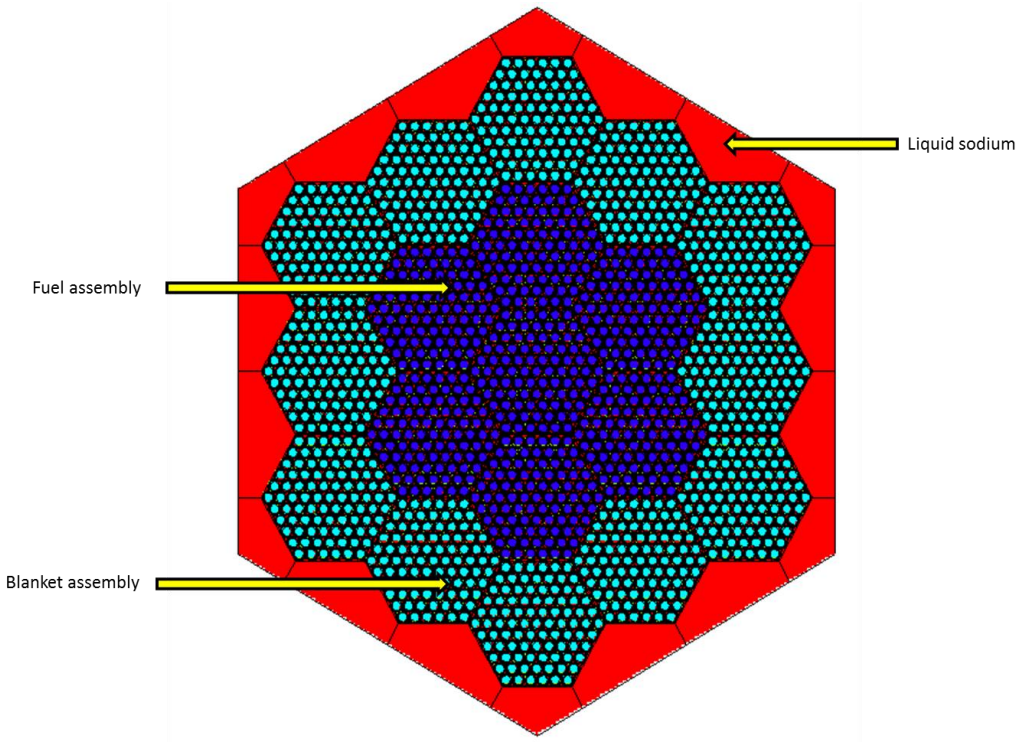

Figure C.2. MCNP model of EBR-II core

APPENDIX D. EBR-II SPENT FUEL ACTINIDE ISOTOPIC COMPOSITION

Actinide	Isotope	wt% in spent fuel
Uranium	233	0.00018%
	234	0.51553%
	235	45.61617%
	236	3.52938%
	238	30.42372%
Neptunium	236	0.00002%
	237	0.15518%
Plutonium	238	0.03487%
	239	14.21843%
	240	4.04938%
	241	1.00041%
	242	0.28871%
Americium	241	0.15516%
	242	0.00047%
	243	0.01128%
Curium	242	0.00017%
	243	0.00002%
	244	0.00086%
	245	0.00003%